Interplay of positive structural inversion and salt tectonics: The case study of the central Algerian margin, Western Mediterranean

Gaia Travan [a,*], Virginie Gaullier [a], Jacques Déverchère [b], Bruno C. Vendeville [a,1]

[a] Univ. Lille, CNRS, ULCO, IRD, UMR 8187, LOG, Laboratoire D'Océanologie et de Géosciences, F59000 Lille, France
[b] Geo-Ocean, Univ Brest, CNRS, Ifremer, UMR6538, F-29280 Plouzané, France

A R T I C L E   I N F O

A B S T R A C T

Convergence between African and European plates generates compressional strain, primarily concentrated along the northern African margin. This is testified on the Algerian margin by numerous earthquakes (e.g. Bougrine et al., 2019) and by the presence of active folds and thrusts. Multi-channel seismic reflection profiles from the MARADJA I survey reveal north-verging thrusts rooted below the Messinian units, and the geometries of the Messinian salt structures. This study examines the characteristics of salt tectonics offshore Algiers and Dellys, focusing on the effect of the positive structural inversion of the former passive margin on geometries, timing, and mechanisms of salt deformation. The interpretation of seismic reflection and multi-beam bathymetric data of the MARADJA I survey, along with its comparison with analogue models, allowed us to reconstruct the salt tectonics processes on the margin and to identify the predominant role of a plateau uplift on salt deformation. Early and ubiquitous salt deformation by downbuilding was followed by a major phase of plateau uplift (end of Messinian Crisis), leading to westward gravity gliding and a slowdown of the salt deformation above the plateau. Km-tall salt structures were developed and thick minibasins deposited. Salt tectonics is nowadays active only where the relationship between salt and overburden thickness is favorable.

1. Introduction

The study of salt tectonics and in general of the salt deposits has an important scientific and economic role. It is often strongly connected to oil industry for the capacity of salt structures to trap gas and oil, as seen in the hydrocarbon-rich provinces of the Gulf of Mexico, North Sea and Campos Basin (Gearing et al., 1976; Warren, 2010). Salt deposits are also exploited onland for both food and chemical industry, as in the case of the Realmonte salt mine (Lugli, 1997). Recent research explores the potential of salt basins in term of CO_2 storage to mitigate carbon dioxide emissions in the atmosphere (e.g. Zhang et al., 2022). However, a side effect of the presence of these sealing layers is the potential development of overpressures below the salt, with consequent drilling hazard during both industrial and scientific drilling operations. A detailed reconstruction of salt deformation is necessary to predict the overpressure formation and reduce potential risks.

Salt tectonics often includes various mechanisms occurring concurrently within a salt system, such as gravity gliding, gravity spreading and crustal tectonics. Therefore, the challenge lies in deciphering the

mechanisms of deformation that act in a given study area and their relative influence on the geometries of the interpreted salt structures. Among the factors enhancing salt tectonics, fault reactivation in the basement is known to play a significant role, particularly in cases of positive or negative structural inversion (Tari et al., 2023). This becomes particularly interesting in the case study of the Algerian margin which undergoes a slow positive structural inversion initiated during Plio-Quaternary times (Leffondré et al., 2021 and references therein). However, the presence of the 5.6 Ma halite layer (Messinian Mobile Unit-MU, Lofi et al., 2011b) at the margin toe prevents from a correct imaging of pre-evaporitic sediments (Jones and Davison, 2014; Simm and Bacon, 2014) and acts as a décollement, thereby limiting the possibility to characterize precisely the geometry and role of crustal faults. This makes the role of salt tectonic analysis particularly important in helping to reconstruct the crustal tectonic evolution of the study area. At a regional scale, the salt tectonics of the Algerian Basin has been interpreted in some recent papers (Bellucci et al., 2021; Blondel et al., 2022; Soto et al., 2022), while several other studies were focused on the tectonic contractional reactivation, the process of subduction inception,

* Corresponding author.
  E-mail addresses: gaia.travan@univ-lille.fr, gaiatravan@gmail.com (G. Travan).
[1] Deceased.

and the nature of the crust (Auzende et al., 1972; Déverchère et al., 2005a, 2005b; Domzig et al., 2006; Yelles et al., 2009; Strzerzynski et al., 2010, 2021; Hamai et al., 2015, 2018; Klingelhoefer et al., 2022). While prior research was mostly focused on the regional crustal and salt tectonics, this work aims at analyzing in detail the salt tectonics on the central Algerian margin, and in particular the effect of the presence of an uplifted plateau offshore Dellys and Boumerdès cities on the timing and geometries of salt deformation. We focused our attention on the sediments of the last 5.6 Ma, namely the Messinian Mobile Unit (MU), the Upper Unit (UU), and the Plio-Quaternary sediments (PQ). Our focus included analyzing the geometries of the base and top of the units, layer thicknesses, and internal reflection geometries to decipher the timing and mechanisms of salt tectonics. This was achieved through the integration of geophysical data interpretation and analogue modelling.

2. Geological setting

2.1. Geodynamical evolution of the Western Mediterranean

The Algerian Basin is located in the Western Mediterranean, between Iberia and Africa, and borders to the west with the Alboran Basin and to the east with the Ligurian-Provençal Basin (Fig. 1). The geodynamical evolution of the Western Mediterranean is the result of the interaction between the African and European plates (Africa, Adria, Europe, and sub-plates) in a context of convergence dated late Cretaceous (Chron C34, 83.5 Ma) (Vergés and Fernàndez, 2012; Macchiavelli et al., 2017), with important influence of the inherited structures (Carminati et al., 2012). Since then, the Africa-Europe plates convergence is going on, possibly interrupted or discontinued by the Paleocene stand-still phase,

which extended up to the Paleocene-Eocene boundary (Schettino and Turco, 2011). The collision between Africa and Eurasia produced extension in the Mediterranean region because it increased the retreat velocity -and consequently the extensional stress- of the African plate in the locked oceanic subduction zone (Jolivet and Faccenna, 2000). This resulted in the diachronous formation of several basins in the overriding plate, the beginning of which has been variously dated between 34 Ma (Gorini et al., 1993), 32 Ma (Carminati et al., 2012) and 30 Ma (Cherchi and Montadert, 1982). In the last decades, many authors shed some light on the geological history of the Algerian Basin, still the most controversial one in the Western Mediterranean in terms of both rifting processes and directions of opening. Three main opening scenarios are proposed by different authors. The conventional model of opening considers that the Liguro-Provençal, the Valencia and the Algerian basins opened in an approximately NW-SE direction, respectively during Late Oligocene-Early Miocene for the first two ones, and during Middle Miocene for the Algerian Basin (Réhault et al., 1984; Schettino and Turco, 2006; Carminati et al., 2012). This would result from an initial N-NW subduction of the Gibraltar-Balearic promontory margin, which is deemed incompatible with the numerical models of the region (Chertova et al., 2014). An alternative scenario considers that this direction of opening would be valid only for the Valencia Basin and the Liguro-Provencal Basin, while an almost E-W opening direction would better explain the observed geometries for the Algero-Balearic Basin (Mauffret et al., 2004; Medaouri et al., 2014). A single NW-dipping subduction zone could have retreated southeastward and subsequently split into two segments, explaining the dual direction of opening (van Hinsbergen et al., 2014). A third scenario suggests the presence of two distinct subducting plates segments for the Alboran and Algerian basins.
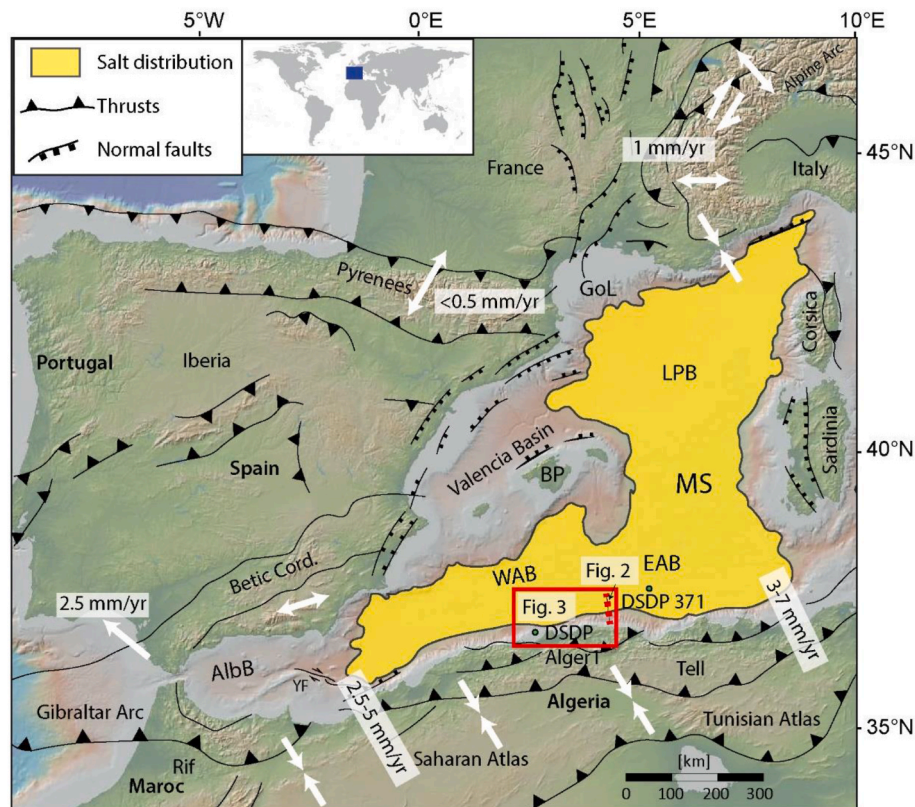

Fig. 1. Present day tectonic map of the Western Mediterranean region with position of the main structural elements and of the Messinian salt deposits compiled from literature (Lofi et al., 2011a,b; Lofi, 2018; Abbassene et al., 2016; Lymer et al., 2018; Jolivet et al., 2021; Stich et al., 2020). The dotted red line shows the position of Fig. 2, and the red rectangle shows the position of Fig. 3. The white arrows indicate the strain regime, and the rate of deformation are from Nocquet and Calais (2004). Figure made with GeoMapApp (www.geomapapp.org)/CC BY (Ryan et al., 2009). AlbB: Alboran Basin; BP: Balearic Promontory; EAB: East Algerian Basin; GoL: Gulf of Lions; Ligurian-Provencal Basin: LPB; MS: Mediterranean Sea; WAB: West Algerian Basin; YF: Yusuf Fault. (For interpretation of the references to color in this figure legend, the reader is referred to the Web version of this article.)

These slabs would respectively dip to SE and retreating to NW, and dip to NW and retreating to SE, nowadays probably separated by a paleo transform fault (Vergés and Fernàndez, 2012). The presence of interpreted detached lithospheric slabs of opposite directions supports this hypothesis (Kumar et al., 2021). Since that time, a two-stage model has been proposed in several works, with some minor differences. These models all suggest a south to south-eastward drift of the AlKaPeCa domain, leading to its consequent collision with the African plate and initiating the detachment of the slab (17 Ma). This was followed by the formation of oceanic crust as a consequence of east-west opening (16-8 Ma) (e.g., Driussi et al., 2015; Aïdi et al., 2018; Leprêtre et al., 2018; Haidar et al., 2022, and references therein). Regardless of which opening model we consider as the correct one, it is likely that (1) the onset of oceanic crust formation in the Algerian Basin is dated at ca. 15–16 Ma (Mauffret et al., 2004; Haidar et al., 2022), i.e. at the end of the Corsica-Sardinia block rotation, (2) oceanic basement formation was almost completed at ca. 10 Ma in the Western Mediterranean, and (3) the extensional strain migrated eastward of Corsica and Sardinia after 10 Ma (Jolivet et al., 2006, and references therein). Consequently, extension stopped in most of the Western Mediterranean, since late Tortonian shortening affected the Western Mediterranean margins (Vergés and Sàbat, 1999). Compressional tectonic reactivation of the margins propagated mostly eastward from the central Algerian Basin (ca. 8 Ma) toward the southern Tyrrhenian Sea (<2 Ma) in a 'scissor-like' pattern, following the subduction cessation, slab tearing propagation and crust-mantle delamination (Jolivet et al., 2006, 2021; Carminati et al., 2012; Booth-Rea et al., 2018a). Once the Western Mediterranean basins were formed, the Messinian Salinity Crisis (MSC) took place between 5.96 and 5.33 Ma (Hsü et al., 1973), resulting in the deposition of a thick sedimentary sequence, isostatic rebound, and significant tilting and subsidence of the sub-basins (see next subchapter for the details).

The relative motion between Africa and Eurasia (i.e. NW-SE oblique convergence) has nowadays a rate that varies between 3 and 7 mm/yr in the Central Mediterranean to 2–5 mm/yr at the western limit of the Mediterranean (Gibraltar Strait) (Nocquet and Calais, 2004; Bougrine et al., 2019) (Fig. 1). This deformation is concentrated at the boundary between Nubia and Eurasia plates, as shown by the seismic activity primarily occurring in a relatively narrow area of coastal Africa (Stich et al., 2006; Ousadou and Bezzeghoud, 2019). The concentration of the stress and strain, and consequently of the mostly reverse fault-type earthquakes, is likely related to the sharp transition between oceanic and continental lithospheres, where the strength is predicted to be lower than in neighbouring regions (Nocquet and Calais, 2004; Hamai et al., 2015, 2018; Auzemery et al., 2021).

2.2. The Messinian Salinity Crisis (MSC)

Tectonic, glacio-eustatic and precession events resulted at 5.96–5.33 Ma into restricted water exchanges between the Mediterranean and the Atlantic Ocean (Hsü et al., 1973). This geological event had a vast impact in the Mediterranean basins, in terms of sedimentary sequence and subsidence rates (Ryan et al., 1973; Réhault et al., 1984) and salt tectonics (Maillard et al., 2003; Obone-Zue-Obame et al., 2011; Gaullier et al., 2014; Lymer et al., 2018). Numerous studies have been conducted on the onset of the Crisis and its causes (Nesteroff, 1973; Selli, 1973; Manzi et al., 2005; Booth-Rea et al., 2018b), on its timing and on its final stages (e.g. Andreetto et al., 2021). For the purposes of this study, i.e. the interactions between salt and crustal tectonics, the CIESM and Briand (2008) consensus chronostratigraphic model provides a sufficiently accurate framework. A first sea lowering and consequent evaporitic deposition in marginal basins started at 5.96 ± 0.02 Ma and led to the deposition of the first evaporites, i.e. the Lower Unit/LU offshore (Lofi et al., 2011a, 2011b) and the primary Lower Gypsum onshore. This event was followed by an estimated sea-level drop of 1500 m around 5.6 Ma (Hsü et al., 1973; CIESM and Briand, 2008), resulting in the formation of the Messinian Erosion Surface (MES). This surface is

diachronous and polygenic, formed by subaerial and subaqueous erosion and carbonates dissolution (Savoye and Piper, 1991; Cornée et al., 2008; Lofi et al., 2005, 2011a, 2011b; Roveri et al., 2014; Maillard et al., 2020). Erosion, together with the slope instabilities resulting from the sea-water drop, led to the deposition of clastic bodies at the foot of the slopes. These units mark the transition between the MSC deposits domain and the MES domain, and are labelled as Complex Unit/CU (Maillard et al., 2006; CIESM and Briand, 2008; Lofi et al., 2011a, 2011b; Granado et al., 2016). The clastic sand deposition is still debated in terms of timing. Some argue that it coincides with the peak of the Crisis (Gorini et al., 2015), while others date it at the onset of the Crisis (Granado et al., 2016).

The strong decrease in the sea level resulted into the precipitation of central basin evaporites (Hsü et al., 1973; Ryan et al., 1973; CIESM and Briand, 2008 and references therein). The thick layer of evaporites is mainly composed of ductile halite and was consequently named Mobile Unit/MU Fig. 4(Lofi et al., 2011b). The marls and evaporites that characterize the last phase of the Messinian Salinity Crisis (5.55–5.33 Ma) (Ryan et al., 1973) testify for water dilution and cyclic salinity fluctuations during the deposition of the Upper Evaporites/Upper Unit and Lago Mare (Orszag-Sperber, 2006; Lofi et al., 2011a, 2011b; Andreetto et al., 2021). The Zanclean reflooding that marks the end of the Messinian Salinity Crisis has been dated differently by various authors: 5.48 Ma (Clauzon et al., 2008), 5.46 Ma (Bache et al., 2012) or 5.332 Ma (CIESM and Briand, 2008). Its duration is also varying significantly: between less than 1000 years (Hsü et al., 1973), few thousands of years for the lighter flood, and less than two years for the final megaflood (Garcia-Castellanos et al., 2009). The important volume of sediments deposited during the Messinian Salinity Crisis increased the subsidence in the basins, enhancing the isostatic adjustment that has already shaped the basin since the beginning of oceanic accretion (Réhault et al., 1984). Moreover, the sea-level drawdown induced a large isostatic rebound, and the Zanclean reflooding induced tilting and subsidence followed by a late regional isostatic uplift (Govers et al., 2009; Rabineau et al., 2014; Heida et al., 2022).

2.3. The Algerian margin

Located in the southern part of the Algero-Provençal Basin (Fig. 1), the Algerian margin is a steep continental margin, reactivated in compression because of the Africa-Europe convergence (Auzende et al., 1975; Déverchère et al., 2005b, 2022). The continental platform is narrow and the continental slope is cut by the two main canyons of Algiers and Dellys (Fig. 3a), draining respectively the Isser and Sebaou rivers (Domzig et al., 2006; Strzerzynski et al., 2010; Cattaneo et al., 2010).

The Ocean-Continent Transition (OCT) on the Algerian margin is extremely narrow with a width generally less than 10 km, distinguishing this margin from other Western Mediterranean margins formed in a similar context and leading to the previously mentioned hypothesis of a multiphase formation of the margin west of Algiers: a rollback of the Tethyan subduction zone, a transcurrent episode and a compressional reactivation (Leprêtre et al., 2013; Haidar et al., 2022). The nature of the crust, interpreted as a thin oceanic one from wide-angle seismic data (Klingelhoefer et al., 2022), is however debated due to the lack of samplings; in the area off Greater Kabylia, it has a thickness range of only 3–5.5 km and is characterized by thickness changes, typical of basins of back-arc settings (Leprêtre et al., 2013; Aïdi et al., 2018).

Another peculiar characteristics of the central Algerian margin, which differentiates this margin from other ones in the Western Mediterranean, is the landward inclination of the top of the Messinian sediments, with the same south-dipping trend of the basement top (Strzerzynski et al., 2010; Leprêtre et al., 2013). This could be the result of the compressional reactivation of the margin or of crustal flexure due to sediment loading (Leprêtre et al., 2013; Hamai et al., 2015). Auzende et al. (1972, 1975) proposed that the Algerian margin could be in an

early stage of subduction, implying underthrusting of the Alboran and Algerian Basins below the African plate (Frizon de Lamotte et al., 2000). The hypothesis of an early stage of subduction has been supported by many recent studies that localized the subduction inception in the central and eastern Algerian margin (e.g., Yelles et al., 2009; Hamai et al., 2015, 2018), where some earthquakes are located below the Moho (Kumar et al., 2021). Although the tectonic reactivation of the northern Algerian margin has been dated at about 8 Ma on land (Recanati et al., 2019), the shortening in the offshore domain is assumed to start later, i. e. during Pliocene or Quaternary times, depending on the margin segment and the distance to the coast (e.g. Kherroubi et al., 2009; Yelles et al., 2009; Strzerzynski et al., 2010, 2021; Déverchère et al., 2022). Note that the margin segment of our study area is made with stiff Hercynian metamorphic rocks of Greater Kabylia and is located at the forefront of the "Maghrebian indenter" (Piqué et al., 1998). This situation may explain why this part of the margin is structurally inverted before the other ones, as supported by geodetic measurements (e.g., Bougrine et al., 2019). In the westernmost margin, a sequential restoration of the stratigraphic evolution across the margin and deep basin provides a calculated peak of the shortening rate higher than 4.5 mm/yr at 5.33–5.42 Ma (Soto et al., 2022).

The Algerian margin currently presents a shortening rate of about 4 mm/yr in NNW to NW strike (Bougrine et al., 2019) (Fig. 1), responsible for destructive earthquakes such as the 2003 Mw 6.8 Boumerdès earthquake displaying a ENE-striking, S-dipping thrust fault (Yelles et al., 2004; Déverchère et al., 2005b; Ayadi et al., 2008; Mahsas et al., 2008; Kherroubi et al., 2017) (Fig. 2 and 3a). On the central Algerian margin, up to 50% of this deformation is supposed to be concentrated in the offshore domain, where Déverchère et al. (2005a, 2005b, 2022) and Domzig et al. (2006) identified a series of 20–35 km long fault-propagation folds forming an uplifted plateau (Fig. 3a) and resulting into the presence of assumed piggy-back basins. These south-dipping structures are accommodating a significant part of the Africa-Europe convergence (Bougrine et al., 2019; Déverchère et al., 2022) and extend over ca. 100 km in a strike sub-parallel to the coastline (Déverchère et al., 2005b; Domzig et al., 2006, Fig. 3). In our study area, the cumulative uplift rate of these crustal structures is estimated at 1.6 ± 0.7 mm/yr, with a northernmost bathymetric scarp of around 300–400 m (Déverchère et al., 2005a, 2022). At a regional scale, active faults at the margin toe (Fig. 2) appear to be segmented but are connected westward and eastward to the Yusuf active transpressional fault (Fig. 1) and to reverse faults of the Sardinia Channel, respectively (Billi et al., 2011; Leffondré et al., 2021, and references therein).

Due to the high reliefs of the Tell-Atlas belt, the main rivers of the area display high availability of sediment supply with seasonal variability (Dan-Unterseh et al., 2011; Giresse et al., 2009, 2013). Additionally, the presence of canyons and the instability of the margins led to the deposition of numerous sedimentary bodies at the foot of the slope (Domzig et al., 2009; Cattaneo et al., 2010; Babonneau et al., 2012, 2017). The generally limited size of these sedimentary bodies is supposed to be linked to the relatively high frequency of earthquakes in the area, supporting their potential role in the triggering of turbidity currents (Ratzov et al., 2015). However, the nature, age and consequent relationship with the Messinian sedimentation remain poorly defined

(Dan-Unterseh et al., 2009; Déverchère et al., 2005b). One prominent bathymetric feature in the area is the Algiers Ridge (Fig. 3 ; 3°–3°30 E), whose deep structure consists of the coalescence of two anticlines (Babonneau et al., 2017), overlain by a sedimentary body resulting from the sedimentation of the Algiers Canyon (Dan-Unterseh et al., 2011).

3. Geophysical data interpretation

3.1. Data and methods

The "MARge Active el DJAzaïr" MARADJA I cruise was carried out by French and Algerian teams onboard the R/V "Suroît" (IFREMER, France) in 2003 (Déverchère, 2003). The scientific survey was aimed at imaging the Algerian margin between Oran and Dellys (1°30 W to 4° E), with both multibeam bathymetric and multi-channel seismic reflection data. During the MARADJA I survey, the multichannel seismic reflection profiles were acquired with two different configurations. More than 4000 km of 6-channels seismic profiles were acquired using as an energy source two double-chamber gas injection air guns shots, with 12 s shots intervals for a total of 93,000 shots. The 800 km of 24-channels seismic profiles were acquired with six double-chamber gas injection air guns shots, for a total of 62,000 shots with 5 s intervals, leading to higher resolution and lower penetration of the seismic data due to the higher frequency of the seismic signal. Consequently, the 6-channels seismic profiles offer a lower resolution image of the Plio-Quaternary sequences but provide a deeper penetration, making them more useful for the imaging of the Messinian sequence. Conversely, the 24-channels seismic profiles offer very high resolution in the Plio-Quaternary sequence but cannot adequately image the evaporitic sequences due to their lower penetration. All the seismic reflection profiles shown in this paper are 6-channels ones.

In this study, we focus on the area offshore Algiers and Dellys cities (Fig. 3), where the density and position of the seismic reflection profiles are particularly interesting for the salt tectonics study. Around 2500 km of seismic reflection profiles of the MARADJA I survey, in an area of more than 9000 km^2, constitute the main dataset for this work and all the profiles shown in the figures (Fig. 3b). Five seismic reflection profiles of the ALE survey from TotalEnergies (Mauffret, 2007) and two profiles of the SH survey from SONATRACH (Cope, 2003) complement the seismic data coverage in the study area (Fig. 3b).

We based our seismic data interpretation on the characteristics of the Messinian deposits described in literature (CIESM and Briand, 2008) and the nomenclature by Lofi et al. (2011a and 2011b) (Fig. 4), as well as the information of wells DSDP site 371 (37°35.8′N, 05°14.55′E) (Hsü and Montadert, 1978) and ALGER1 (36°46.30′ N; 2°44.21′E) (position in Fig. 1, Burollet et al., 1978). The interpretation of the seismic reflection data was performed using Kingdom™ software from IHS Markit, and the grids were calculated with Kingdom™ software and Golden Software Surfer®. All the maps presented in this paper are generated using the mathematical modelling flexgridding algorithm. Comparable results were obtained using the data adaptive gradient projection algorithm, except for artifacts related to interpolation around salt diapirs, resulting in unnatural geometries. In practice, it is beneficial to create maps using both methods during the study, bearing in mind that both algorithms
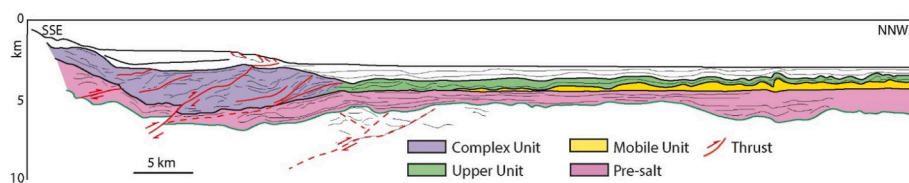

Fig. 2. Line drawing of a regional depth section representative of the study area, where the main sedimentary units and deep thrust ramps are evidenced. The green line represents the basement top. The section is located off Greater Kabylia, just east of the study area (see Figs. 1 and 3 for location). Modified after Leffondré et al. (2021). (For interpretation of the references to color in this figure legend, the reader is referred to the Web version of this article.)
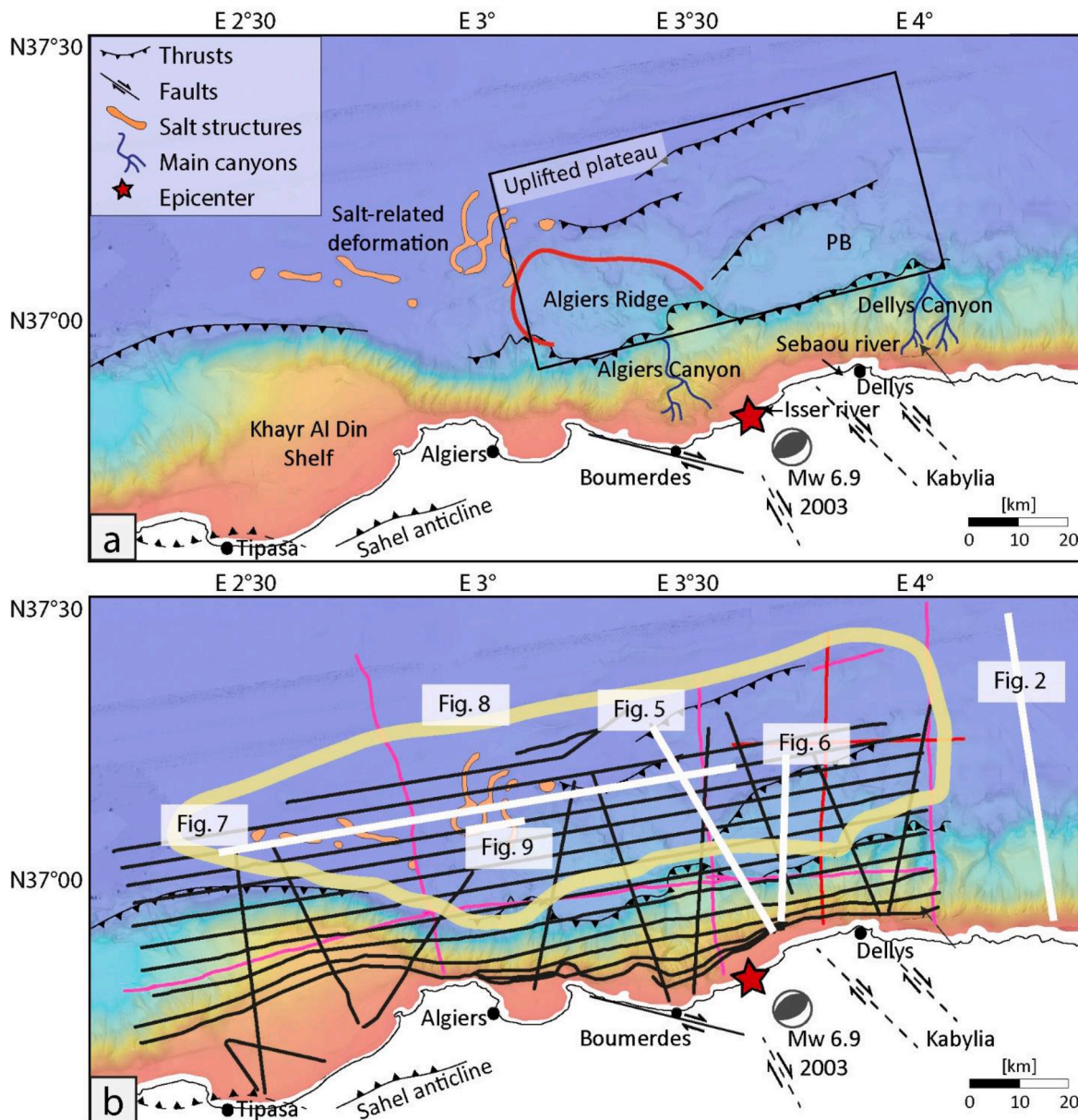
Fig. 3. The Algerian margin. a. Detail of the study area bathymetry from the MARADJA survey (2003) and position of the main structural elements compiled from literature (after Déverchère et al., 2005a,b; Domzig et al., 2006; Babonneau et al., 2017; Bougrine et al., 2019). Part of the salt-related deformation in the area is visible on the bathymetry and is highlighted in orange, while the uplifted plateau is marked by the black rectangle. The limit of the Algiers Ridge is marked in red. PB: Piggyback Basin b. Position of the regional line drawing and of the seismic reflection profiles used for this study in relation with the main structural elements position: MARADJA I (black lines), SH (pink lines) and ALE (red lines). The position of the line drawing and seismic profiles shown in this paper is underlined in white, while the position of the grids presented in Fig. 8 is marked in yellow. (For interpretation of the references to color in this figure legend, the reader is referred to the Web version of this article.)

may introduce inaccuracies and their sole purpose is to illustrate trends.

During the MARADJA I survey, high resolution multibeam bathymetry has been acquired through the Simrad Kongsberg EM300 multi-beam echosounder. This system operates at a frequency of 32-kHz and consists of 135 beams for a total aperture of 140° and horizontal planes antennas. It provides a swath coverage of 5 times the water depth, with a lateral resolution of 25–35 m at 1000 m depth and a vertical accuracy of 2–10 m. The system is efficient up to a water depth of 4000 m (Domzig et al., 2006). The EM1000 system, operating at higher frequency of 95 kHz, with 60 beams and a total beamwidth of 150° using circular antennas, is designed for shallower waters (0–1500 m) and has been employed to image the sea bottom on the continental platform. The Digital Elevation Model (DEM) used in this work was constructed after

processing with CARAIBES IFREMER Software, and has a maximum grid spacing of 50 m. The bathymetric data in the Algerian margin have been particularly useful as a complement to the seismic reflection data because both salt tectonics and crustal tectonics are still active in the area, therefore affecting the seafloor geometries.

3.2. Geophysical data interpretation results

We present here the results of the seismic and bathymetric data interpretation, starting with the seismic stratigraphy and then focusing on the salt tectonics and salt-related structures. Due to the focus of this work and the limited data penetration, the seismic interpretation primarily concentrates on the Messinian Mobile Unit and Upper Unit and
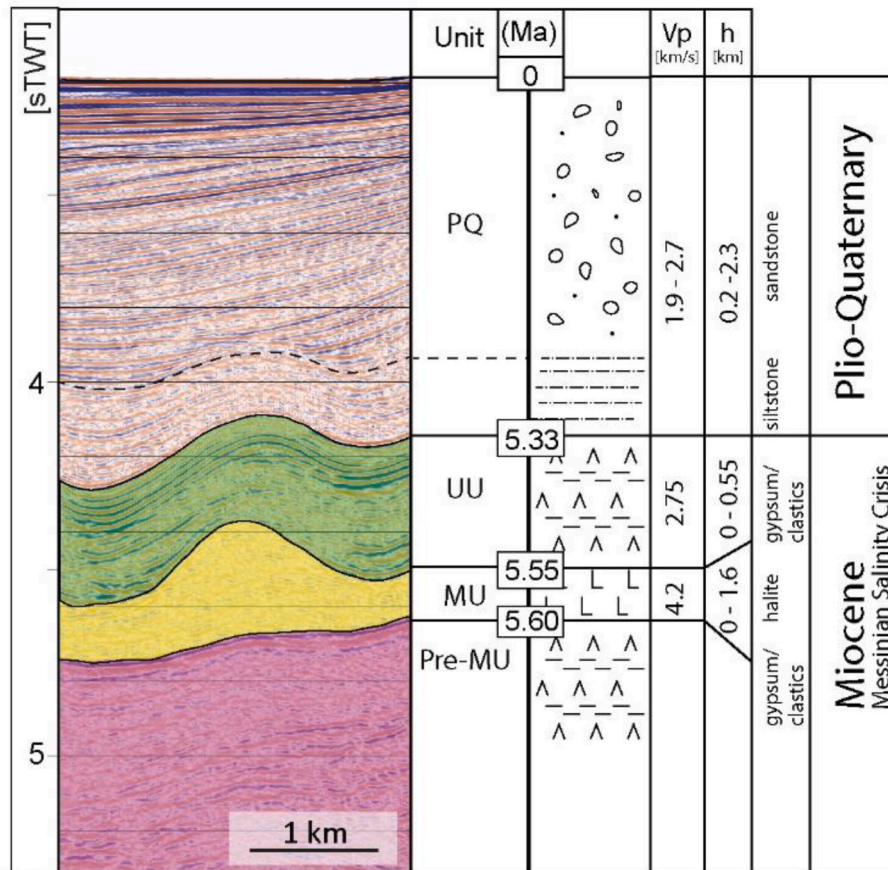
Fig. 4. Detail of seismic profile MARADJA 01–97, with the seismostratigraphic units interpreted in the dataset, correlated to the simplified synthetic stratigraphic column of the Messinian and Plio-Quaternary sediments of the Algerian margin (after CIESM, 2008; Lofi et al., 2011a). Seismic velocities (Vp) from literature (Leprètre et al., 2013; Camerlenghi et al., 2020; Soto et al., 2022) have been used to calculate the average thickness (h) of the interpreted seismic units. PQ: Plio-Quaternary; UU: Upper Unit; MU: Mobile Unit. See text for details.

the Plio-Quaternary sediments. Locally, mainly in correspondence with salt welds, we were able to image pre-salt sediments geometries.

3.2.1. Seismic stratigraphy

Pre-salt sediments (> 5.6 Ma): The imaging of pre-evaporitic sediments is made difficult by the presence of the evaporitic layer, which has a shielding effect on the seismic signal, as previously mentioned. Where they are imaged, typically below the salt welds or in correspondence with the thinnest salt layer, the pre-salt sediments present low to medium amplitude and low-frequency continuous reflections, often deformed by the pull-up effect caused by the high seismic velocity of the salt (Fig. 4). These reflectors are consistent with the Lower and Middle Miocene marly and likely detrital sequence, with an open-sea depositional environment in the upper part (Réhault et al., 1984). At least the upper portion of this sedimentary sequence is presumed to be the Lower Unit (LU), deposited at the beginning or immediately after the major drawdown of the MSC and composed of clastics sediments (Lofi et al., 2005) and/or evaporites (Krijgsman et al., 1999). Due to the uncertainties regarding the presence and thickness of the LU in the area and the characteristics of the seismic signal, we will refer to the sediments pre-dating the Mobile Unit as 'pre-salt'.

The Mobile Unit (MU, 5.6–5.55 Ma): Deposited at the peak of the MSC and mostly composed by halite (Hsü et al., 1973), the Mobile Unit (MU) is the central topic in this study, and its geometries will be described with more details in the next section. The interpretation of the shape of the salt is often limited by the complex travel path of the seismic waves across salt structures (Jones and Davison, 2014). It has a calculated interval velocity of 4.2 km/s in the Western Mediterranean

(Camerlenghi et al., 2020), slightly lower than the 4.5 km/s of the pure halite. This seismic sequence is seismically transparent (Fig. 4) with sporadic reflections caused by the deposition of chemically and physically different evaporites and the incorporation of clastic layers during salt tectonics (Lofi et al., 2011b; Dal Cin et al., 2016; Granado et al., 2016). The base of the MU is imaged in the seismic reflection data as a negative polarity horizon (Figs. 4–6), consequence of the generally lower acoustic impedance of the pre-salt sediments. The reflection amplitude of this reflector is medium to very low due to the shielding effect of the salt layer on the seismic signal. The top of the MU appears as a continuous positive reflection of high amplitude, owing to the very high velocity of the seismic waves in the halite and the consequent strong difference of acoustic impedance between the MU and the UU (Fig. 4). Local difficulties in the interpretation are due to salt tectonics and the consequent local verticalization of this horizon, therefore hardly imaged in the data (Fig. 5). The thickness of the MU varies between 0 (salt welds) and 1.6 s TWT, so up to 3.3 km calculated thickness.

Upper Unit (UU, 5.55–5.33 Ma): This seismic unit characterizing the end of the MSC is composed of marls and evaporites, and presents a calculated interval velocity varying between 2.5 and 2.75 km/s (Soto et al., 2022) and 3.5 km/s (Camerlenghi et al., 2020). In our dataset, the UU presents a seismic facies of continuous, high-amplitude reflections, creating a strong contrast with the underlying MU and with the lower amplitude, continuous reflections of the overlying lower Pliocene (Figs. 4 and 5). Its thickness varies between 0 and 0.4 s TWT, i.e. between 0 and 0.55 km, and pinches out towards the south (i.e. landward). Considering the short-wavelength variations in the UU thickness, it is challenging to evaluate the thickness of the UU at a regional scale.
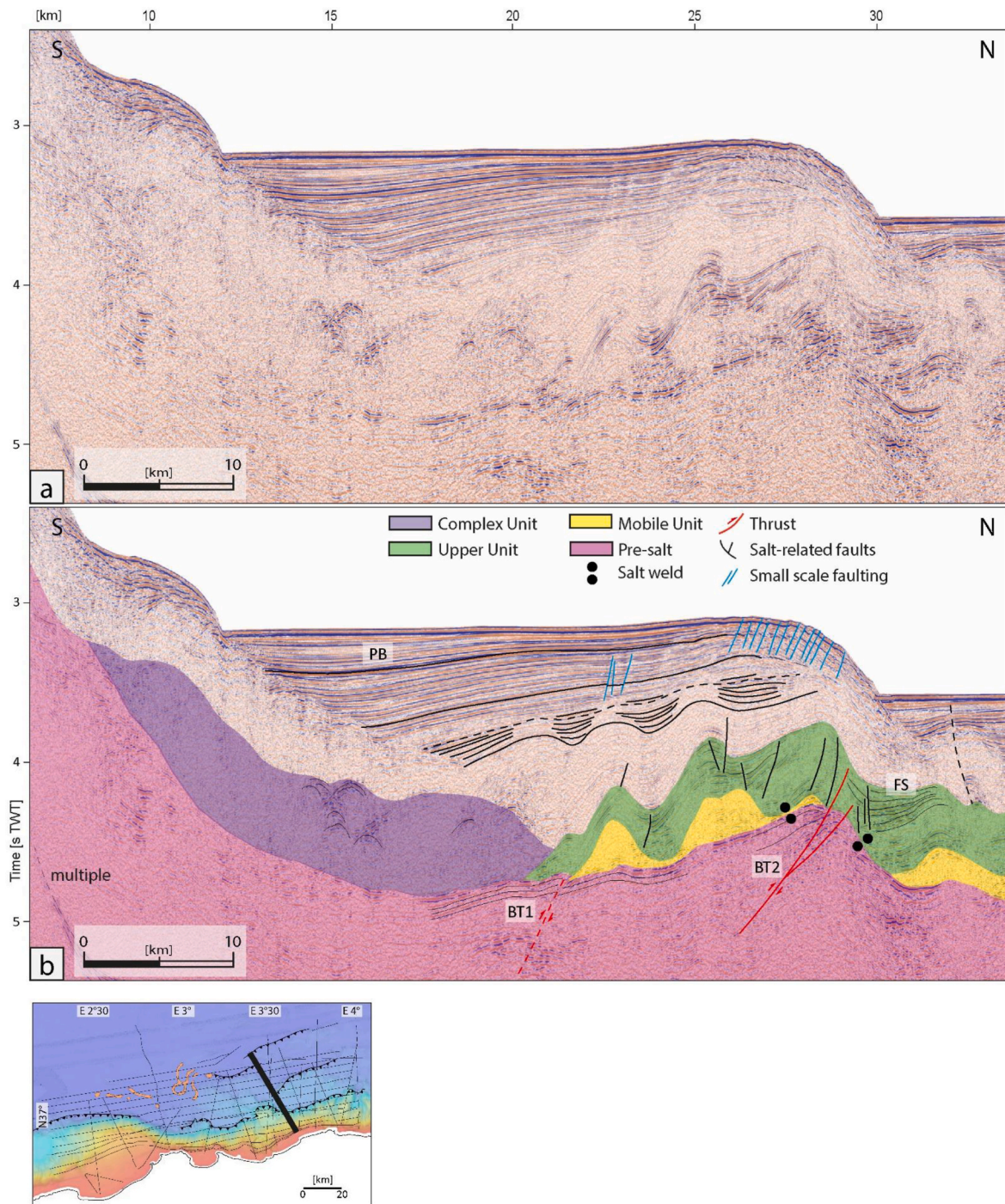
Fig. 5. Seismic profile MDJ01-96, perpendicular to the margin and crossing the uplifted plateau (position in Fig. 3b). a. Uninterpreted b. Interpreted. The black dotted line divides the Plio-Quaternary sediments into two seismic sequences: a lower sequence in which are co-present the effects of the salt and crustal tectonics and an upper one in which the horizons geometries are exclusively the result of the thrust activity. VE at the seafloor: 5.6 X. BT: Blind Thrust, FS: FanShaped strata; PB: Piggyback Basin.

However, its thickness does not exhibit a clear trend of change, except for a slight thinning that correspond to the thrusts positions.

Complex Unit (CU): This unit is located at the foot of the margin and displays a mostly chaotic seismic facies (Lofi et al., 2011a). The horizon marking the base of the CU becomes, towards the basin, the base of the MU, while its top is approximately in continuity with the top of the UU (Figs. 5 and 6). The lateral limit between CU and UU is marked by the transition from chaotic seismic facies to one composed of parallel medium-amplitude horizons. While the base of this unit seems to be coeval with the beginning of the salt deposition (Fig. 5) the vertical transition between CU and Pliocene can be difficult to track because of the very low amplitude reflectors of both seismic facies (Figs. 5 and 6). Due to its seismic facies and its stratigraphic position, this unit is believed to represent the offshore prolongation of reworked flysch units from onshore central Algeria (Aïdi et al., 2018).

Plio-Quaternary (PQ, 5.33–0 Ma): As a consequence of the re-established marine conditions at the end of the Crisis, the Plio-Quaternary (PQ) sequence is mainly composed of marly sediments, as evidenced by the sedimentary sequence recovered in the wells. In the DSDP well 371, the cores are composed of calcareous mud and
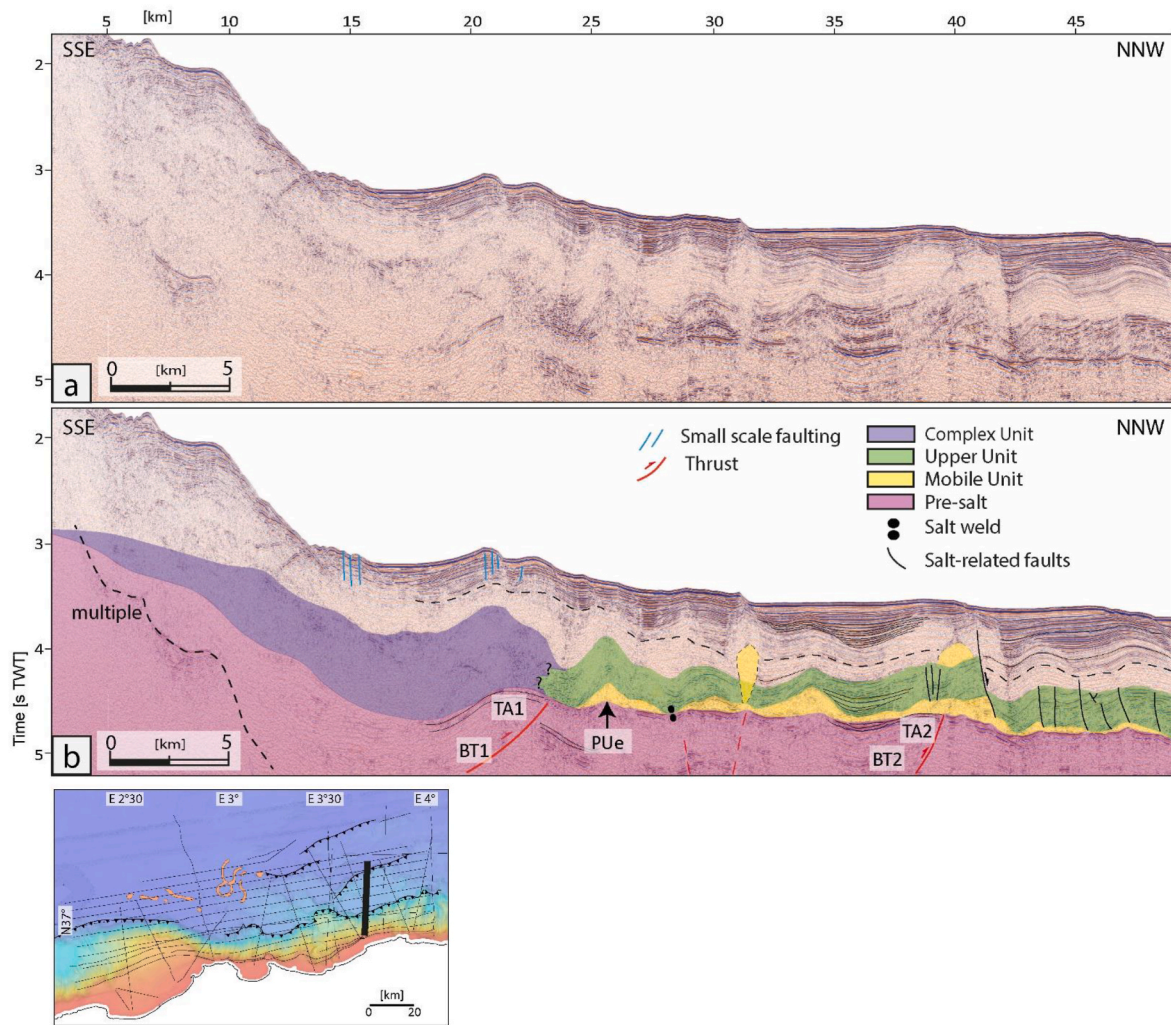
Fig. 6. Seismic profile MDJ01-95, perpendicular to the margin and crossing the uplifted plateau (position in Fig. 3b). a. Uninterpreted b. Interpreted. VE at the seafloor: 5.6 X. BT: Blind Thrust, TA: Thrust Anticline, PUe: Pull-Up effect.

mudstones, while in the ALGER1 well, sand, sandstones with marls intercalations, and gray plastic marls are reported (Burollet et al., 1978). During the Lower Pliocene, deposition consists of pelagic and hemipelagic clays and becoming turbiditic during the Upper Pliocene with the deposition of sand and clays (Réhault et al., 1984). This results in a semi-transparent Lower PQ characterized by low amplitude and continuous reflections. The semitransparent facies of the Lower PQ sometimes makes it difficult to visualize these horizons and their geometries, preventing us to accurately date salt movement during early Plio-Quaternary times. During the Upper PQ, the reflection strength increases while maintaining the same frequency, and the reflection geometries are locally wavy, indicating the detrital and coarser nature of this most recent part of the sequence. The seismic velocity of the PQ unit strongly depends on the depth, as these is a direct proportionality between sediment compaction and seismic velocity. On the Algerian margin, the calculated V_p varies from 1.9 to 2.7 km/s (Leprêtre et al., 2013) or from 1.9 to 2.2 km/s (Soto et al., 2022).

The trend of the PQ sedimentary thickness is characterized by thicker deposits near the coast line, with maximum values of around 1.7 s TWT (i.e. 1.6–2.3 km depending on the velocity used for the conversion), and reduced values going towards the center of the basin, away from the influence of the river sedimentary supply. Fan-shaped strata characterize most of the PQ unit (e.g. Fig. 5), while infilling geometries are more common in the most recent sediments (e.g. Fig. 7). We can observe both in the seismic profiles (Fig. 7c) and in the bathymetric data (Fig. 3)

the formation of sedimentary minibasins surrounded by salt structures, which will be described with more details in the salt tectonics subpart below.

3.2.2. Uplifted plateau and salt-related structures

As documented in literature (Déverchère et al., 2005a,2005b), the area is characterized by the presence of thrusts resulting from the reactivation in compression of the margin. These thrusts, and in general the geometries resulting from compression, are clearly visible in some seismic profiles roughly perpendicular to the margin and to the thrusts (Figs. 5 and 6). Seismic profile MDJ01-96 (Fig. 5) shows a blind thrust (BT1 in Fig. 5) deforming the pre-salt sediments and predating the deposition of the UU. A second blind thrust (BT2 in Fig. 5) uplifts the salt base horizon, resulting in the formation of a southward slope of calculated 4° and in the formation of a step in the base MU horizon. While the UU has a relatively constant thickness in the area, the presence of this step results in a lateral thickness variation of the UU and the formation of fan shaped strata in the upper part of this unit (FS in Fig. 5), testifying a phase of activity of this thrust. In Seismic Section MDJ01-95 (Fig. 6), we can interpret the effect of a blind thrust (BT1 in Fig. 6) on the geometries of late Miocene to Plio-Quaternary sediments, forming a thrust-related anticline (TA in Fig. 6). Another blind thrust is interpreted (BT2 in Fig. 6), and above it, a NNW directed normal fault rooted in the MU offsets the UU and partly the Plio-Quaternary. In addition to the deformation due to the thrusts activity, the UU and PQ also present
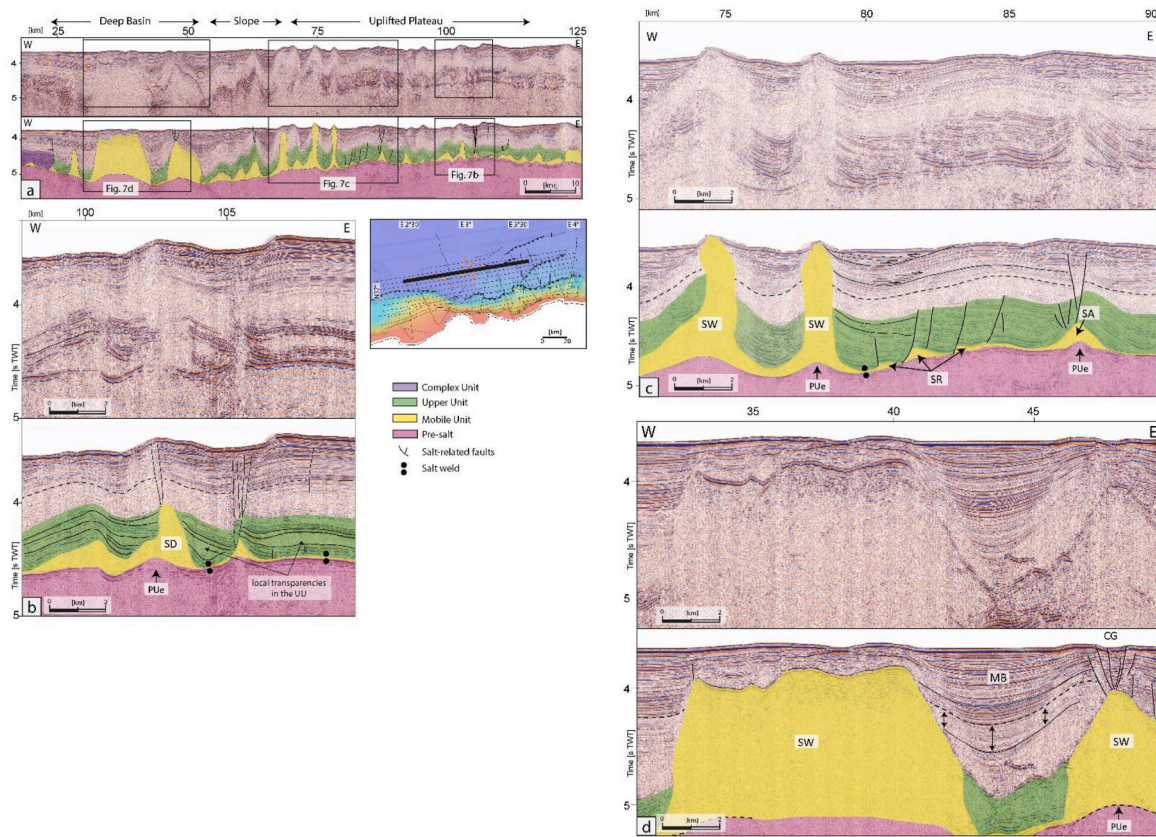
Fig. 7. a. Seismic reflection profile MDJ01-03, parallel to the margin offshore Algiers and Boumerdès, uninterpreted and interpreted (position in Fig. 3b). The black rectangles marks the position of Fig. 7b, c and 7d. VE at the seafloor: 8.8X. b. Detail of seismic profile MDJ01-03 located on the uplifted plateau. VE at the seafloor: 5.6X. c. Detail of seismic profile MDJ01-03 located on the slope, at the transition between the uplifted plateau and the deep basin. VE at the seafloor: 5.6X. d. Detail of seismic profile MDJ01-03 in the deep basin, imaging the major salt structure of this study area. VE at the seafloor: 5.6 X. CG: Crestal Graben; MB: Mini-basin; PUe: Pull-Up effect; SD: Salt Diapir; SR: Salt Roller; SW: Salt Wall.

shorter wavelength anticlines that are likely related to salt tectonics.

Seismic data interpretation highlighted that, together with the presence of the uplifted plateau, the area presents a marked division for what concerns the geometry of the Mobile Unit (Figs. 7, 8a and 8b). This division is well visible in seismic profile MDJ01-03 parallel to the margin (Fig. 7), where we can observe the different salt structures that characterize the uplifted plateau to the east (3°10 E to 4°E, Fig. 7b), the westward slope (2°50 E to 3°10 E, Fig. 7c), and the deeper sector to the west (2°20 E to 2°50 E, Fig. 7d). To provide a clearer illustration of the geometries of each sector, we will describe the uplifted plateau, the slope and the deeper area separately. We also propose some approximate depth conversion for the two-way travel time (TWT) thicknesses and depths interpreted in the data. These conversions serve as rough estimates and should not be regarded as precise indications of structural localization.

a. **Uplifted plateau.** Between 3°10′ and 4°E, the uplifted plateau is characterized by values of depth of the MU base between 4.1 and 4.7 s TWT, roughly convertible in 3.6–4 km depth, with shallower values correlating well with the position of the blind thrusts offshore Dellys and Boumerdès (Déverchère et al., 2005a; Domzig et al., 2006) (Fig. 5a, 6 and 7). In correspondence with the major salt structures, the base of the salt appears deformed due to the pull-up effect (PUe in Fig. 8) caused by the high seismic velocity in halite, and the seismic signal is often cancelled or very disturbed (Fig. 7). The top of the MU is also lifted at a shallower position (average 4.5 s TWT, roughly convertible in 3.8 km depth) and reaches values as shallow as 3.8 s TWT, roughly convertible in 3.25 km depth (Fig. 8b), while the salt structures are limited both in terms of number and of development

(Figs. 5, 6 and 7b). In this sector the salt diapirs, salt anticlines and salt rollers generally reach heights up to 200–300 ms TWT, equivalent to a few hundreds of meters in thickness, and are separated by 2–3 km of thin salt or salt welds (Figs. 5, 6 and 7b). Numerous salt-related faults offset the UU and early PQ (e.g. Figs. 5 and 6). A few salt diapirs reach a thickness of 500 ms, i.e. slightly more than 1 km (Fig. 7b). The internal reflections in the UU show slightly fan-shaped strata while they are truncated and uptilted in correspondence with the salt diapirs and deformed above the anticlines (Fig. 7b). Moreover, a seismic transparent layer of 120 ms TWT thickness is observed in the UU in this area (Fig. 7b), suggesting the presence of a salt layer. This salt layer could be either salt migrated from the MU beneath or autochthonous salt resulting from a locally shallower environment. During Plio-Quaternary, the synkinematic depositional geometries that could be related to salt tectonics are minimal and mostly restricted to the scarce salt diapirs above the uplifted plateau. This is particularly evident in the seismic profiles perpendicular to the thrusts, where we can distinguish different levels of deformation (Fig. 5b): the UU displays salt-related anticlines, while the early Pliocene is also characterized by a southward thickening, a geometry typical of piggy-back basins (Strzerzynski et al., 2010). This is followed by a thin sequence of onlapping reflectors, followed by piggy-back geometries without any influence of salt tectonics.

b. **Westward slope:** The slope at the western limit of the uplifted plateau (2°50 E to 3°10 E, Fig. 7c) marks a sudden change in the MU geometries. The base of the salt deepens westward between 4.6 s and 5.4 s TWT depth over a span of 45 km, forming a calculated average gradient of 2.6°. The transition between the uplifted plateau and the
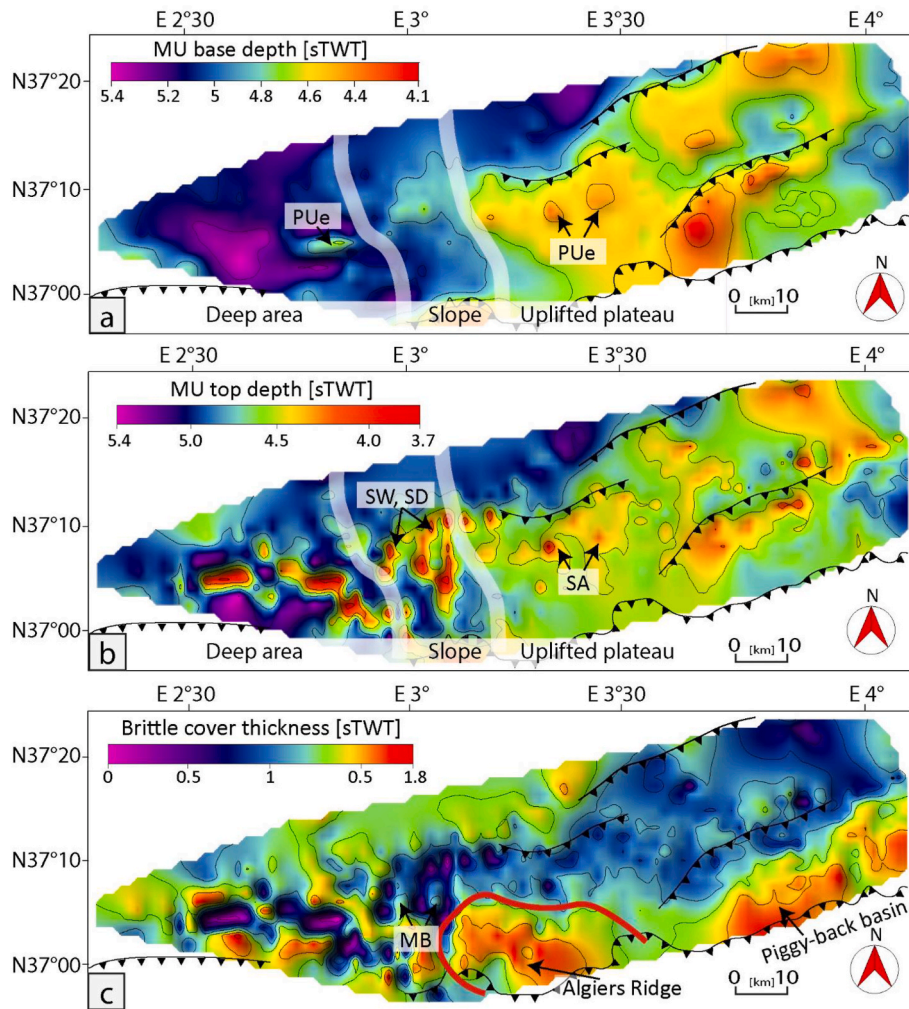
Fig. 8. Isobath maps and thickness map obtained from the seismic data interpretation. Position in Fig. 3b a. Isobath map of the base of the Mobile Unit, with contour lines every 0.2 s TWT and values between 4.1 and 5.4 s TWT. The position of the thrusts is from Déverchère et al. (2005) and Domzig et al. (2006), while the white line shows the division between the uplifted plateau, the slope and the deep area. b. Isobath map of the top of the Mobile Unit on the Algerian margin, with contour lines every 0.4 s TWT and values between 3.7 and 5.4 s TWT. c. Thickness map of the brittle cover, i.e. Upper Unit and Plio-Quaternary deposits, on the Algerian margin with contour line every 0.3 s TWT and values between 0 and 1.8 s TWT. The limit of the Algiers Ridge is marked in red. MB: Mini-basins; PUe: Pull-Up effect; SA: Salt Anticline; SD: Salt Diapir; SW: Salt Wall. (For interpretation of the references to color in this figure legend, the reader is referred to the Web version of this article.)

slope generates an area of extensional salt tectonics, characterized by significantly reduced salt thickness and westward dipping normal faults rooted in the MU and shifting the whole UU. Moving westward on the slope, we encounter an area of well-developed salt structures of up to 1.2 s TWT (i.e. 2.5 km) high, locally affecting the seafloor morphology (Fig. 7c). The inclination of sediments within the depocenter (Fig. 7c) indicates that the growth of the salt diapir to the west is greater compared to that of the salt diapir to the east. Thanks to the high resolution bathymetric data, we can appreciate the 3D extension of these salt tectonics structures (Fig. 9). The salt diapir, up to few km thick as imaged in this seismic profile, corresponds to an annular salt ridge, while the smaller salt structure besides produces a crestal graben well identified on the seafloor. The localized high-amplitude seismic reflections inside the salt body are most likely a lateral reflection of the top of the MU, although they could possibly indicate a layer of brittle sediments incorporated into the salt during ductile deformation. The internal layering of the UU shows lateral thickness variations and onlap geometries, while this unit is absent in correspondence with the salt diapirs, and the onlapping horizons are uptilted around the salt diapirs. The PQ horizons are deformed up to the seafloor, and onlapping geometries are present, while the PQ

deposits are almost absent above the two salt diapirs. The sediment thickness is maximal towards the center of the minibasin and thinner towards the salt structures. Maximum tilting of the seismic reflectors occurs towards the salt structures. The sedimentary sequences between the salt structures are interpreted as polygonal minibasins, characterized by a dish-shaped syncline with diameters ranging from 6.5 to 8 km, subsiding into the salt layer. The area of maximum development of the polygonal minibasins is at a latitude of 37°5′30–37°15′ and a longitude of 2°57′ to 3°6′. The internal area of these minibasins varies between 26 km^2 and 37 km^2.

c. **Deep area:** The average value of the salt base depth abruptly deepens from east to west, reaching depths of 5–5.4 s TWT at 2°40 E (Fig. 8a), i.e. 4.7 km calculated depth. The maximum depth of the salt base is attained at 2°37′N 37°E, where the 5.4 s TWT depth corresponds to one of the shallowest values of the MU top, therefore forming massive salt structures imaged in Fig. 7d which also affect the bathymetry. In this area, the UU thickness remains relatively constant where the salt is undeformed, while it is absent due to erosion or lack of deposition in correspondence with the massive salt diapirs and salt walls. Since the thick brittle cover (UU and PQ) reaches here its maximum values of 1.8 s TWT (i.e. almost 2 km), and
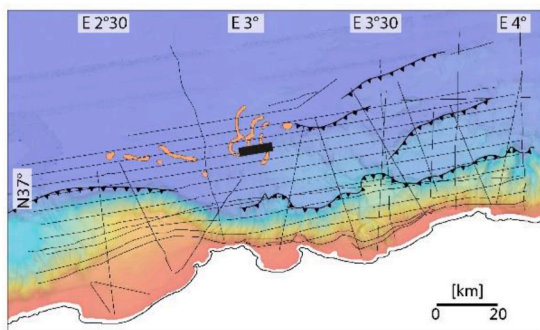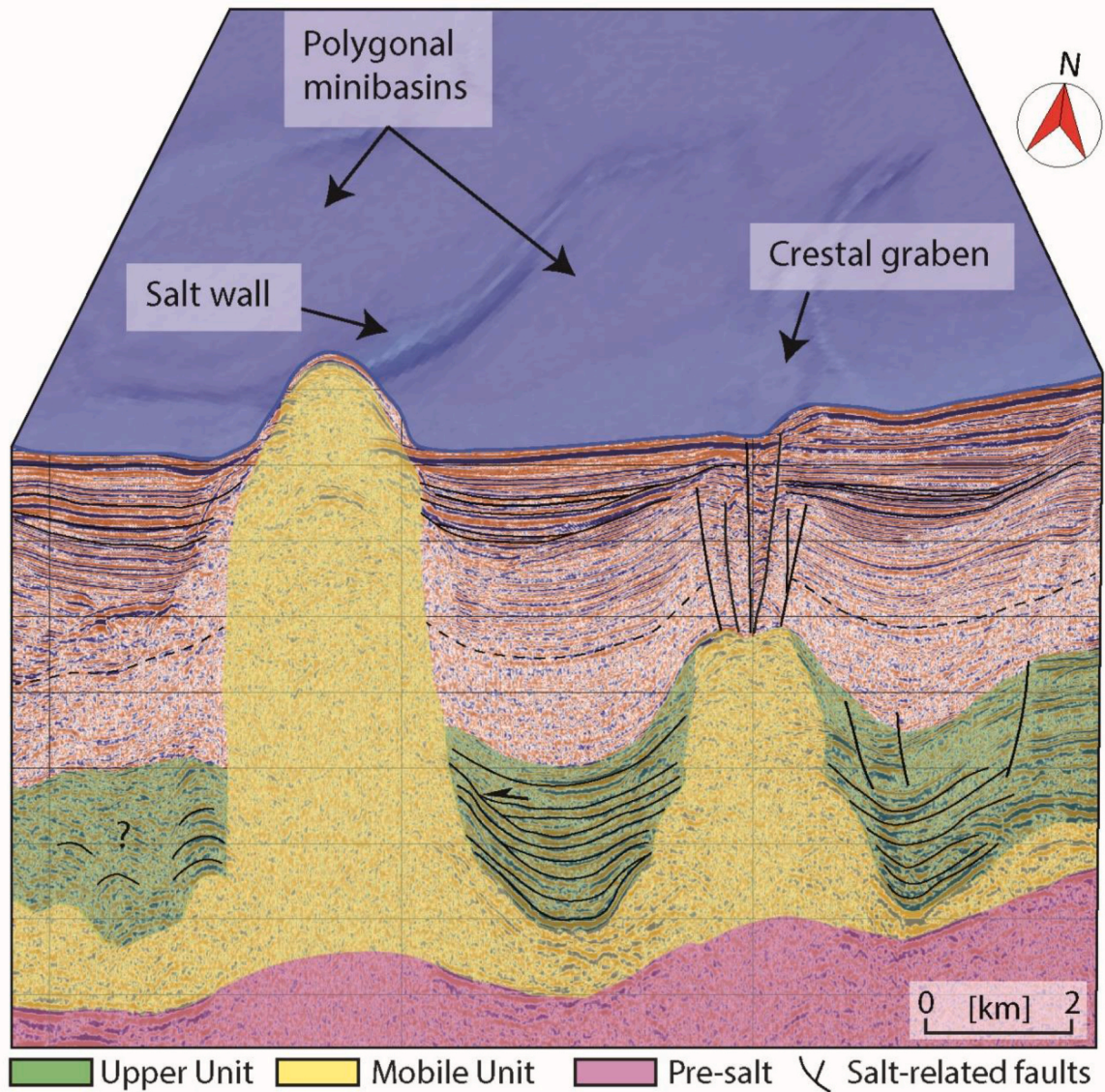
Fig. 9. Detail of seismic profile MDJ 01–04, parallel to the margin and imaging the salt mini-basins, and of the multibeam bathymetry data of the MARADJA survey. Position in Fig. 3b. VE at the seafloor: 6.7X

because numerous lateral reflections are present there, we cannot evidence growth strata in the UU. Between the salt walls, the PQ unit thins towards the salt structures and forms typical geometries of the salt minibasins already described on the slope.

Brittle cover (Fig. 8c): From a mechanical point of view, the Upper Unit and the PQ sediments can be considered as a single sedimentary sequence, defined as the brittle cover as it is characterized by brittle deformation, in contrast with the ductile behaviour of the MU. The interpreted thickness of the brittle cover ranges between 0 and 1.8 s TWT (Fig. 8c), that correspond to values between 0 and 2250 m of sediments using an average seismic velocity of 2.5 km/s. The spatial

variations in the brittle cover thickness (Fig. 8c) reveals a maximum thickness of the brittle sedimentary cover near the coastline and two main depocenters of different origins: the eastern one (3°40′ to 4° E) results from syn-tectonic sedimentation during the thrusting activity (piggy-back or perched basins, Fig. 3a–Déverchère et al., 2005a) and corresponds to a local low of the bathymetry, while the one at 3°5′-3°20′ corresponds to the building of Algiers Ridge (Fig. 3a; Babonneau et al., 2017) and is a local high on the bathymetry. Also the MU geometry strongly influences the thickness of the brittle cover, with the lower values of brittle cover thickness recorded above the main salt structures. Small wavelength variations in sediment thickness are related to the presence of salt diapirs, with absence of UU and very limited PQ deposition in correspondence with the largest diapirs and salt walls.

4. Analogue modelling

Following the geophysical data interpretation phase, a comparison was made with the results of scaled analogue models produced in the Analogue Modelling Laboratory Bruno Vendeville, at the Laboratoire d'Océanologie et de Géosciences (UMR 8187), University of Lille (France).

4.1. Rationale for the modelling program

The geometries interpreted in the seismic reflection and bathymetric data revealed a strong contrast between western and eastern sectors of the study area. The eastern area is characterized by the presence of an uplifted plateau of crustal nature (Déverchère et al., 2005a), above which the salt layer is thin and the base and top of the salt are uplifted. A westward slope with a calculated gradient of 2.6° connects this area to the western sector, where the base of the salt is deeper, without signs of crustal activity and with km-thick salt walls. Based on these observations, different sets of models were created to test the influence of the tectonic inversion and the consequent plateau uplift at the margin toe on the salt deformation and how the presence of a salt layer affects the overburden deformation (Lymer, 2010; Besème, 2013; Travan, 2022).

4.2. Analogue materials and scaling parameters

The analogue model is intended to represent in a simplified way and at a smaller space-time scale a natural phenomenon, complying with the similitude rule; relationships of time, space and forces have to be maintained (Hubbert, 1937). While the models are based on the well-established rules of scaling of Hubbert (1937) and adapted by Eisenstadt et al. (1997), certain approximations were necessary due to technical constraints, such as limitations in box model dimensions, or the slightly fluctuating temperature conditions in the laboratory. Additionally, human constraints, like restricted access to the analogue modelling laboratory at night, necessitated limiting the compressional phases of the models to a maximum duration of approximately 12 h.

For all the models presented in this paper, the geometrical similarity is respected and the length ratio $l^* = l_{model}/l_{natural}$ prototype is 10^{-5}, so 1 cm in the model corresponds to 1 km in the natural example (Table 1) (Hubbert, 1937; Schellart and Strak, 2016). The rule of geometric scaling has also been applied to the conversion of interpreted seismic facies thicknesses (i.e., Mobile and Upper Units, and Plio-Quaternary). Considering the ductile nature of the Mobile Unit -and the consequent nowadays high variability of its thickness in the area- there is an uncertainty about the initial thickness of this layer, for which we consider an average value of 1 km of salt (CIESM and Briand, 2008 and references therein), i.e. 1 cm of silicone in our models. A proper volumetric reconstruction would be possible only through basin scale 3D data coverage and corrections for dissolution and erosion. The overburden thickness scaling was based on an average value of the interpreted layers thickness. The simplification applied is compatible with the nature of these layers and the level of approximation that characterize the

Table 1

Properties of the material and scaling parameters of our models. DI: Density Inversion between the salt and its overburden. See text for the details.

Parameter	Equation	Model	Natural prototype	Scaling ratio (model/nature)
Length l		1 cm	1 km	$l^* = 10^{-5}$
Sand/overburden density ρ (no DI)		1 g/cm³	2.2 g/cm³	$\rho^* = 0.45$
Sand/overburden density ρ (DI)		1.2 g/cm³	2.6–2.7 g/cm³	$\rho^* = 0.45$-0.5
Silicone – salt layer density ρ		1 g/cm³	2.2 g/cm³	$\rho^* = 0.45$
Gravity		9.8 m/s	9.8 m/s	$g^* = 1$
Viscosity μ of silicone and salt		μ = 10^{18} Pa·s	μ = 10^5 Pa·s	$\mu^* = 10^{-14}$
Deviatoric stress	σ = ρ·g·l			$\sigma^* = 5 \cdot 10^{-6}$
Strain rate	$\gamma^* = \sigma^*/\mu^*$			$\gamma^* = 5 \cdot 10^8$
Time	$T^* = 1/\gamma^*$	1 h	57,000 years	$T^* = 2 \cdot 10^{-9}$

analogue models. To simulate the ductile behavior of the salt rock (viscosity μ = 10^{17}–10^{19} Pa·s, LeCompte (1965) we use a near-Newtonian polymer of viscous silicon PDMS polydimethylsiloxane with a μ = 10^5 Pa·s at room temperature. Consequently, μ^* = μ model/μ natural prototype = 10^{-14}. The halite has a density of around 2.2 g/cm³, while the silicone used has a density of around 1 g/cm³ giving a ρ^* = ρ model/ρ natural prototype = 0.45, that can be approximated to 0.5 (Hubbert, 1937). An uncertainty regarding the physical characteristics of silicone arises due to the use of recycled silicone, which contains a very small percentage of sand, particularly fine one. In fact, to mitigate the environmental and economic impact of analogue modeling, the silicone used in our finished models undergoes sedimentation to separate the silicone from the sand, enabling its reuse across multiple models. This does not seem to impact strongly its physical characteristics, even if our tests are limited to verifying the spreading behavior of the new and recycled silicon putties.

Quartz sand of 125–315 μm grain size and a density of 1.2 g/cm³, an angle of internal friction around 30°, and negligible cohesion, replicate the brittle behavior of the rocks. Vertical and lateral variations of the overburden densities are unknown and are thus not considered in our models. Considering the variability in literature regarding the presence or absence of density inversion between the Messinian salt and its overburden in the Western Mediterranean, and given that we have established ρ^* = around 0.5 in our scaling, in some of the initial models (Lymer, 2010), the absence of density inversion between the salt and the Plio-Quaternary sediments was assumed, and therefore, a combination of fine sand (ρ = 1.2 g/cm³) and PVC powder (ρ = 0.8 g/cm³) was used to achieve a density of 1 g/cm³. Conversely, if we consider the presence of a slight density inversion (e.g., in Soto et al., 2022, the density of the UU to PQ sequence has a range between 2.66 and 2.72 g/cm³), sand alone is sufficient, more manageable, and less impactful in terms of waste production.

No gravity acceleration (g) is applied on our models, so g^* = g model/g natural prototype is 1 (Hubbert, 1937). The driving forces in our models are the tectonic stresses (models compression) and the vertical loading produced by the layers of modelling materials. On the other side, the resisting forces are the frictional strength of the sand and the viscosity of the silicone.

We can calculate the deviatoric stress imposed on the model σ^* = $\rho^* \cdot g^* \cdot l^*$ = 0,5·1·10^{-5} = $5 \cdot 10^{-6}$, so the stresses endured by the Algerian margin are 5,000,000 times greater than those in our experiment. We can thus calculate the shear tectonic stress: σ^* = $\gamma^* \cdot \mu^* \Leftrightarrow \gamma^* = \sigma^*/\mu^*$. Therefore, γ^* = $5 \cdot 10^{-6}/10^{-14} = 5 \cdot 10^8$. Therefore, 1 h of deformation in the model corresponds to 500,000,000 h in nature, which is approximately 57,000 years, giving a scaled duration of almost 100 h for the model. This value provides an order of magnitude, and considering the

approximations made during this calculation, our deformation will occur at a rate of 1 cm/h. To overcome this issue related to a calculated modeling duration of almost 100 h, an initial acceleration (5 cm/h) of the plateau uplift is applied in models sets 2 and 3. This initial acceleration allows us to finish the rest of the model with a scaled velocity of 1 cm/h.

4.3. Experimental setup and procedure

The experimental setup consists of a salt-bearing margin in which the reactivation in compression led to the formation of an uplifted plateau, indicated by the presence of a series of thrust rooted beneath the Messinian salt. The uplift of the plateau has a clear influence on the development of the salt structures, and therefore models are created to assess its impact on the area.

The experimental program has been carried out at the Bruno Vendeville Analogue Modelling Laboratory (LOG, UMR 8187 - University of Lille) and includes 3 sets of analogue models for a total of 6 models setups summarized in Table 2. The models were produced between 2010 and 2022 during internships and theses supervised by the authors of this paper, and never object of a peer-reviewed publication.

The experimental deformation box comprises a flat horizontal plane metal base, three lateral fixed glass walls of 20 cm height and 9 mm thickness to resist pressure, and a mobile wooden wall. The length of the panels varies slightly among the different sets of models, with an average size of 90 × 60 cm (Fig. 10). The mobile wall allowed compression of the experimental space for models 1C, 2 and 3 through a worm-screw propelled by a motor. The motor velocity is controlled and changed via software. In the models sets 2 and 3, a rigid plate measuring 25 × 45 cm is positioned on the southeastern portion of the box bottom. This placement is intended to establish a preferential zone for simulating crustal deformation and plateau uplift, as interpreted from the seismic dataset, by directing compression effects toward the northern region of the box. The first set of models (Table 2, Lymer, 2010) considered a layer of silicone with 4 cm thick sand lobes on top. In the first model (Table 2, Model 1 A), the salt base was uniform, while in the second (1 B), a sand plateau was constructed to model the effect of the reactivation in compression of the margin through passive deformation of the silicone and sand layer. In the third model of this set (Table 2, Model 1C), the effect of compression was added, albeit without continuous uplift of the plateau, thus differing from the real scenario.

Starting from model set 2 (Besème, 2013), we transitioned to models with density inversion between the salt (silicone) and its overburden, along with a distinct division between a zone with and without silicone. Additionally, from this moment onward the uplifted plateau is formed using a rigid plate, as previously described (Fig. 10). The sedimentary sequence (Fig. 10c) comprises several layers of sand below the silicone layer, the presence of a silicone layer in part of the box model (Fig. 10a), and a scaled thickness of sand layers modelling the salt overburden deposited during the modelling. Different sand colors allow to better identify the deformation and faulting in the modelling material. In total, sand thickness ranging from 1.6 to 2 cm was added in the depocenters, and approximately 1 cm elsewhere on the model with variations related to the model's topography. On top of each layer, a very thin layer of microbeads is added using a stencil to create a grid with squares

measuring 1.5 cm on each side. This allows us to better observe the deformation of the model's surface. Concerning model set 2, a 6-h compression phase at a velocity of 1 cm/h to create the uplifted plateau was followed by 19 h without compression, during which deformation results from lithostatic pressure and gravitational acceleration. During these 19 h, no sedimentation is added. Starting from model set 3 (Travan, 2022), after a faster initial compression to initiate the formation of the plateau, compression was adjusted to 1 cm/h, compatible with both the scaling of the deformation of the area and with the timing of silicone deformation. In Model 3 A, after the 6h40′ of model compression, we slowed down the velocity to 0.2 cm/h, and let the model deform for 15 h without sedimentation. In Model 3 B, localized depositions of the Plio-Quaternary layer were added to simulate future minibasin depocenters, despite not strictly reflecting the casual deposition of sediments. This simplified approximation allowed for accelerated modeling while ensuring silicone structures' growth. While the thickness of each layers is based on the geometrical scaling, the sedimentation rate is partly adjusted to constantly assure silicone structures growth while avoiding silicone extrusion.

During the modelling sets 2 and 3, thin slices of silicone have been removed from the northern and western walls of the box, to accommodate model deformation.

To monitor the surface and lateral deformations of the experiments during the different phases of modeling, time-lapse high-resolution digital photographs are taken at 5 min intervals for the 3 sets of models. In particular, the surface view is useful to compare the model surface to bathymetric data and to have a partial 3D image of the evolution of the model. Due to the lateral effect (i.e. friction of box walls etc.) side view data are not strictly representative of the situation in the model. At the conclusion of each experiment, the cutting process involves N–S and E–W sections every 2–3 cm, to obtain the maximum amount of information possible. Section placement was guided by observed minibasins structures at the model surface during the modelling procedure. Each section is immediately photographed with high-resolution cameras to document the produced geometries.

4.4. Analogue modelling results

In this section, we briefly summarize the results of the three sets of models, with a particular focus on Model 3 B (Figs. 10 and 11, Table 2), which contains the largest number of elements useful to understand the salt tectonics in the study area, and whose procedure has been defined based on the results of previous models (sets 1 and 2, Table 2).

In Model 1 A (Lymer, 2010) radial and concentric faults formed as a result of the sedimentation of sand lobes above the silicone layer. These geometries have been previously described in Gaullier and Vendeville (2005) as characteristic of gravity spreading salt tectonics. In Model 1 B, the presence of the constructed uplifted plateau results in significant vertical and horizontal redistribution of silicone, and consequent deformation of the overburden. The addition of N–S compression in Model 1C results into partially inhibited deformation in that direction, and the silicone structures have a slight tendency towards N–S orientation. Regarding the analogue models sets 2 and 3, we observe that the compression and the presence of a basal plate below the sand and silicone sequence resulted into the development of a series of thrust and an

Table 2

Summary of the experimental program with the main differences between the models sets. For the details, see text.

| Models set	Synthesis		NS Compression	Plateau uplift	ρ inversion
1 – A, B, C	Sedimentary lobes	A -Pure gravity spreading	absent	absent	absent
		B- Sand built plateau below silicone	absent		
		C - Sand built plateau plus compression	present		
2	Homogeneous overburden layers. Phase of compression followed by phase of lithostatic pressure plus gravity		present	present	present
3 – A, B		A - Phase of compression followed by phase of lithostatic pressure plus gravity	present	present	present
		B - Localized sedimentation (minibasins seeds)	present		
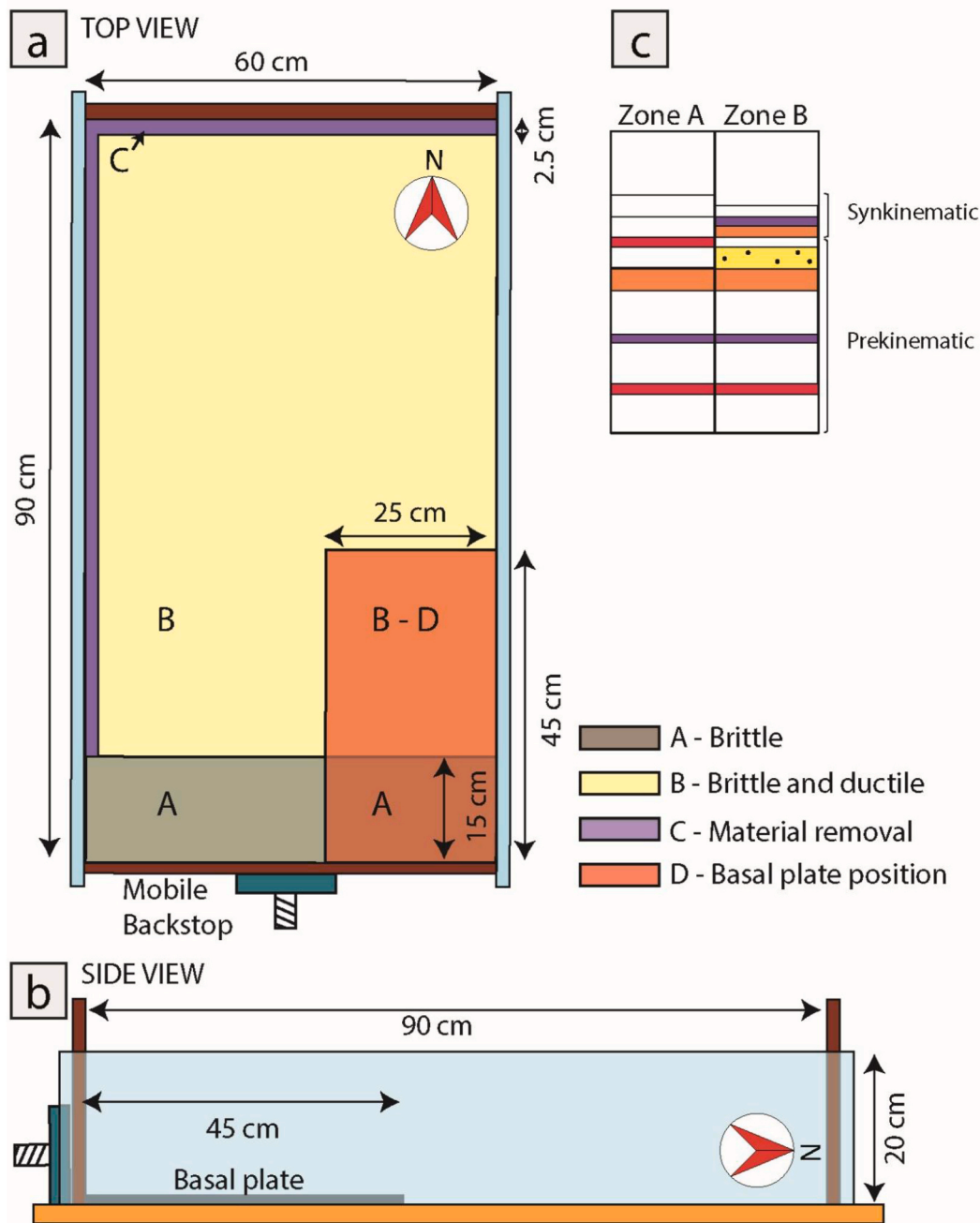
Fig. 10. Schematization of the experimental setup in top view (a) and side view (b). The division in different areas is based on the nature (brittle vs ductile) and thickness of sediments and on the actions that will be performed during the experimental procedure. c. Schematic representation of the sand and silicone (dotted yellow) thickness in zone A and B at the beginning of the experiment set 3. For details, see text. (For interpretation of the references to color in this figure legend, the reader is referred to the Web version of this article.)

uplifted plateau on the eastern side of the model, and the formation of normal faults in the brittle overburden (Fig. 11a). While the faults array is quite complex, we can recognize preferential E-W and N–S directions at the northern and western edges of the uplifted plateau, respectively. Several faults and grabens at the northern and western limits of the box model can be considered as edge effects. In both Models 2 and 3 A, the phase of N–S compression (velocity 1 cm/h) was followed by a phase in which deformation occurred for an extended period of time (15–19 h) without sedimentation and with absent or limited compression (0.2 cm/h). Minibasins formed naturally on the model without localized sedimentation from our part, and are mostly present on the slopes

surrounding the uplifting plateau. This allowed us to confirm the formation of salt minibasins even with an overburden of laterally consistent thickness, thus prompting us to artificially induce minibasin formation in order to expedite model run times for Model 3 B.

Concerning the result of Model 3 B (Fig. 11), we can divide it into two phases; during the early stages of the experiment (T = 0 to T = 5h30') the major deformation visible on the model consisted in the deformation related to the uplift of the plateau in the eastern part of the model, as well as the formation of folds result of the compressional deformation, and mostly N–S normal faults at the western limit of the forming plateau. As the model developed, polygonal minibasin geometries and associated
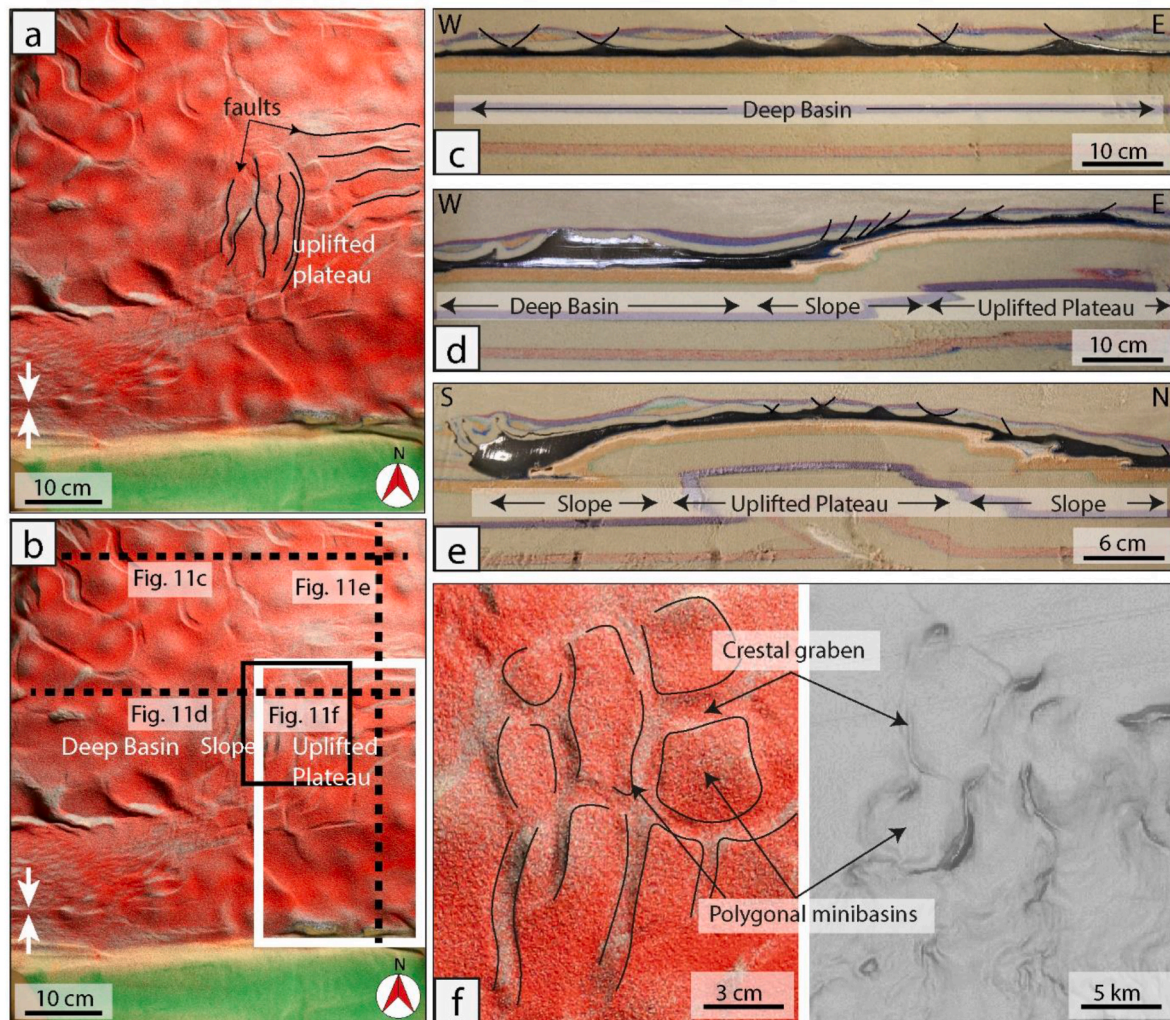
Fig. 11. Results of the analogue model 3 B of the area. a. Top view of model 3 B at the end of the model, with interpreted faults and well visible the mini-basins geometries. b. Top view of model 3 B with position of the following images. White rectangle: position of the uplifted plateau. Black dotted lines: positions of Fig. 11c, d and 11e. Black rectangle: position of Fig. 11f c. E-W section of the analogue model at 6.5 cm from the northern limit of the box. d. E-W section of the analogue model at 25.5 cm from the northern limit of the box, crossing the uplifted plateau. e. N–S section of the analogue model at 8.4 cm from the northern limit of the box, crossing the uplifted plateau. f. Zoom of the minibasins geometries visible on the model surface (on the left) and comparison with the seafloor geometriesseen in Fig. 8 (on the right).

crestal grabens became clearer and are particularly well-developed at the western edge of the uplifted plateau, and the N–S and E–W faults are well defined above plateau (Fig. 11a,b,f).

The internal geometries at the end of Model 3 B have been observed in the cut sections. In the E-W sections, a section cut in the northern part of the model (Fig. 11c) displays a homogeneous distribution of salt anticlines and salt-related normal faults outside the area of influence of the uplifted plateau, with ubiquitous minibasins dividing the few cm thick salt diapirs. In the sections cutting through the uplifted plateau (Fig. 11d) we observe above the plateau geometries of extensional tectonics and reactive diapirism, i.e. reduced silicone thickness, silicone anticlines with crestal grabens, and silicone related normal faults. On the slope, in correspondence with well-formed minibasins geometries on the model surface, silicone diapirs are separated by depocenters mainly thinning towards the plateau. The silicone layer, homogeneous at the beginning of the experiment, is thinner above the uplifted plateau and thicker towards west, where it forms diapirs and silicone walls up to several cm thick. In all the observed sections, the pre-kinematic sand layer of the overburden (Fig. 10c) becomes stepper towards the major silicone structures, testifying a deformation that is mostly result of "salt" tectonics. Downbuilding is shown by synkinematic depocenters, with onlapping geometries towards the silicone structures.

In the N–S sections (Fig. 11e), the effect of the northward and southward slopes is well visible, with thin-skinned extensional faults indicating gravity gliding towards north and towards south consequence of the plateau uplift. Above the uplifted area the silicone is thinned (0.1–0.7 cm) and forms silicone anticlines and small diapirs, with geometries characteristic of reactive diapirism. Normal faults cut the sand overburden, testifying that the silicone deformation continued up to the end of the model. Thicker silicone is located both northward and southward. The main difference between the two downslope areas is the fact that southward the silicone is stopped by the brittle sedimentary layer of zone A and forms therefore several cm thick silicone structures, while northward it has more space to migrate and form salt anticlines. The minibasins geometries recognized on the model surface corresponds in the cut sections to sand depocenters thinning towards the plateau and surrounded by silicone diapirs.

5. Discussion

Thanks to seismic data interpretation, bathymetric data and wells information, we have completed a detailed and systematic study of the

geometry of the Messinian salt layer and its overburden at the toe of the central Algerian margin. While very limited imaging of the pre-salt horizons is available, the Messinian salt and brittle overburden display outstanding structures which are particularly significant to understand the causal link between salt and crustal tectonics on the Algerian margin. By integrating seismic reflection and bathymetric data, a comprehensive 2.5D interpretation of the salt structures has been achieved, enabling to reconstruct the deformation history in this peculiar area, subjected to a compressional stress arising from the slow-rate Africa-Eurasia convergence and from its position at the northernmost tip of the plate boundary. The observed geometries led to the hypothesis that the tectonic uplift of the basement triggered an E-W gravity gliding of the salt layer, with consequent formation of extensional faults and associated salt rollers (Fig. 7c), a thinning of the salt above the uplifted area and an accumulation of salt downslope, where salt diapirs of up to 3 km calculated thickness can form. The different factors acting through time and determining the final geometries observed have been analyzed here through analogue modelling, which led to a better understanding of the mechanisms at the origin of these structures. We discuss below the specific role of crustal tectonics, propose a sequential evolution to explain the structures reported, and finally speculate on the factors at the origin of the formation of the minibasins.

5.1. Effect of crustal shortening on messinian salt tectonics

Since the MSC occurrence, salt and crustal tectonics are acting together along the Algerian margin, resulting into a challenging reconstruction of the different deformations interpreted in the area. Indeed, the slow-rate crustal deformation in compression can be partly accommodated by the salt movements and consequently the timing of crustal tectonics is concealed. Thanks to the interpretation of the seismic reflection and bathymetric data, and the comparison with the produced analogue models (Fig. 12e and f), we analyze here the mechanisms of salt tectonics and its interaction with crustal tectonics in an area of more than 9000 km^2, and reconstruct the temporal evolution of the salt and its overburden deformation.

Numerous seismic profiles - parallel and perpendicular to the margin - image the area offshore Algiers and Dellys. This data density allows us to obtain detailed grids of the different Messinian surfaces (Fig. 8), and in particular of the base and top of the salt. In these grids, we observe a marked division between eastern and western parts. On the one hand, above the eastern tectonically uplifted plateau, where the base and the top of the MU are deformed and uplifted, the thickness of the salt is limited and the salt structures have a vertical development mostly limited to few hundreds of meters. The Plio-Quaternary deposits are around 700 m thick but are spread in a wide range, between 100 ms TWT above the major salt structures and 1.4 s TWT around them, and present growth strata related to the tilting of piggy-back (perched) basins in the middle and lower continental slope (Déverchère et al., 2022). The salt tectonics stops prematurely here due to the N–S compression. On the other hand, the western sector is not affected by crustal tectonics, and the base of the salt is deeper (Fig. 8a). The thick salt layer forms there major salt structures of 1.5–2 km height, and well developed salt walls are still deforming the seafloor, as shown in the bathymetry (Fig. 3a). The two areas are connected by a gentle slope, with intermediate characteristics in terms of salt and overburden thickness and still active salt deformation visible on the seafloor (Fig. 3a and 9). The complexity of the area analyzed has given rise to several questions, mainly concerning the timing of the plateau uplift and the role of the crustal tectonics on the salt movement. A pre-MSC uplift of the plateau could not be excluded a priori, because due to the limits in the imaging of the pre-salt sedimentary sequence, syn-kinematic geometries could have been possibly missed. Analogue modelling cannot provide a solution to this uncertainty, but the normal faulting interpreted in Fig. 7a and 7c evidences that part of the salt previously located above the plateau moved westward, partially explaining the differences in the MU

thickness between the uplifted plateau and the deeper area. Owing to the ductile nature of this layer, it is however impossible to estimate the initial amount of salt initially deposited in the two sectors. Therefore, the difference in salt thickness between western and eastern sectors can be either the consequence of a differential deposited thickness or a post-plateau uplift salt migration, or both.

Considering the regional long term tectonic evolution of the area and the significant vertical motions produced by the Plio-Quaternary thrusts in the central Algerian margin (Fig. 2) (Déverchère et al., 2005a, 2022; Kherroubi et al., 2017), we may hypothesize that this salt thickness difference, together with the interpreted geometries of the salt and its overburden and the presence of the plateau, mostly results from an early salt deformation by E-W thin-skinned gravity gliding above the Messinian salt layer, consequence of the plateau uplift. This hypothesis has been analyzed through analogue modelling, where the uplift of the plateau and the silicone layer's response to the uplift were successfully reproduced (Fig. 11), obtaining geometries that are closely resembling the ones interpreted in the geophysical data (Fig. 12e and f).
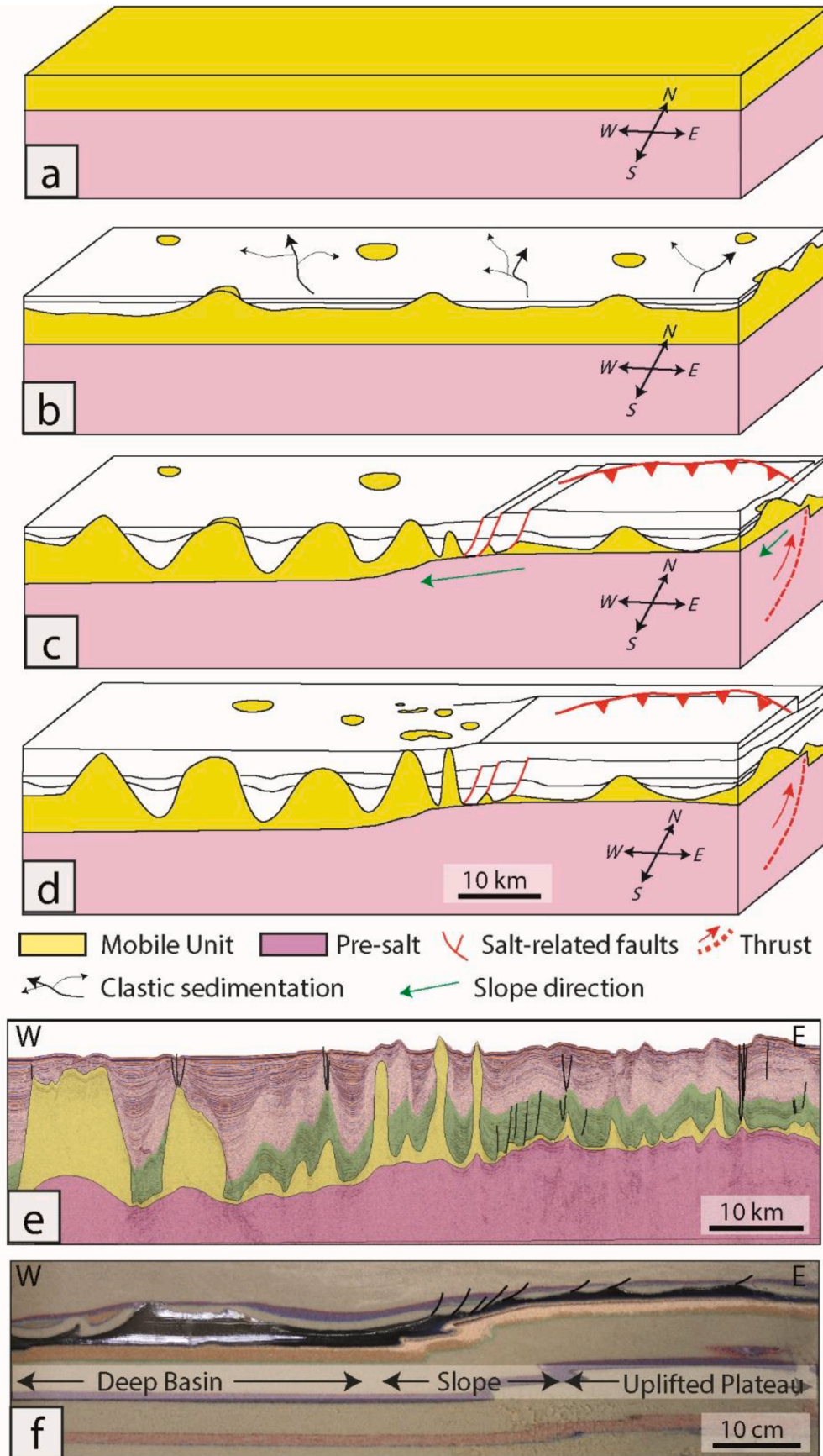
5.2. Evolution of the area

As a result of the integration of geophysical data observations and the analogue models, we propose here a sequential evolution of the study area since the deposition of the Messinian Mobile Unit (MU), i.e. since 5.6 Ma (Fig. 12).

Phase 1 - Deposition of the MU (Fig. 12a): Due to its evaporitic nature, the deposition of the salt cancelled the pre-existing bathymetric differences in the basin; at the end of the MU deposition, the bathymetry is flat. If bathymetric differences existed prior to the salt deposition, these differences in elevation were less than the MU thickness, otherwise onlapping geometries of the UU would have been identified in the area. In analog Model 1 B (Table 2), the model setup considered a plateau uplift predating the salt deposition, but the results in terms of final geometries are not significantly different. It is therefore not possible to determine whether the basement uplift started before, during, or immediately after the deposition of the Messinian salt.

Phase 2 - Downbuilding during the deposition of the lower UU (Fig. 12b): The analysis of the depositional geometries, and in particular from the growth geometries in the UU (thickness differences, onlapping horizons, Fig. 7b, 6 and 9), indicates that the onset of the salt movement predates the end of the MSC. The differential pressure due to the irregular clastic sedimentation (UU) led to the ubiquitous formation of the first salt anticlines and diapirs that grew for downbuilding in all the area, forming salt-related minibasins geometries. Besides from these small-scale, fan-shaped geometries along the salt anticlines, the lower UU does not display important regional thickness changes, except for the thinning and onlapping on the margin. This suggests a relative absence of intense tectonic activity during most of the UU deposition period.

Phase 3 - Uplift of the plateau (Fig. 12c): The compressional crustal tectonics likely initiated the uplift of the plateau before the end of the MSC, as suggested by the fan-shaped geometries of the UU in seismic profile MDJ01-96 (FS in Fig. 5). The uplift of the plateau resulted in the creation of two directions of local slopes, respectively landward above the plateau (Fig. 5) and westward at the western limit of the plateau (Fig. 7), this last one resulting into early Plio-Quaternary gravity gliding along an area of around 6 km (Fig. 7a and c). The normal faults and associated salt rollers are comparable to the geometries observed in Model 3 B (Fig. 10d), in which the uplift of the plateau led to a redistribution of the silicone, that flows westward towards the deeper area. The major phase of crustal shortening is concentrated during the Quaternary, as evidenced by the across-strike tilting of the piggy-back basins, quite well recorded by the Quaternary sedimentary sequence (Fig. 5, seismic profile MDJ01-96; Déverchère et al., 2022). Actually, during early PQ, the thickening of the sedimentary sequence towards the south is coeval to the formation of salt-related anticlines, highlighting the causal link between crustal and salt tectonics. The salt-related

(caption on next page)

Fig. 12. Schematic reconstruction of the evolution of the Algerian margin between 2°10′ and 4°E during the last 5.6 Ma, based on the results of the seismic data interpretation and analogue modelling. See text for the details. a. The MU deposition flattened the topography. b. While the UU was depositing, the first salt structures formed ubiquitously by downbuilding. c. Before the end of the Messinian Salinity Crisis the eastern plateau started to uplift, leading to gravity gliding westward (green arrow). d. Despite crustal tectonics is still active in the area, recent salt tectonics characterize only the slope and part of the abyssal plain, where the salt walls are thicker. e and f. Comparison between the seismic data interpretation (e) and the results of analogue model 3 B (f). (For interpretation of the references to color in this figure legend, the reader is referred to the Web version of this article.)

anticlines stopped to form quite early, while the slope of the salt base still increased later on, as testified by the typical piggy-back geometries of the PQ and by the step in the bathymetry (Strzerzynski et al., 2010; Déverchère et al., 2022). The approximately N–S directed compression would have prevented NS directed salt gravity gliding and prematurely stopped the salt tectonics above the uplifted plateau.

Phase 4 - Recent evolution (Fig. 12d): As the plateau continues to uplift, a net division between the eastern and western sectors is established, leading to different evolution in these areas. The growth of salt structures by downbuilding persisted in the western sector, while above the plateau the movement stopped due to different factors. Firstly, the salt thickness is limited and the salt welds are common (Fig. 7 and b), preventing the development of salt structures. Additionally, the presence of piggy-back sedimentation exerts a buttress effect on the salt (Fig. 5), contrasting the effect of the increased slope due to crustal tectonics that could have led to gravity gliding southward. Nowadays, salt tectonics is primarily active on the slope at the western limit of the plateau, in correspondence with the polygonal minibasins which formed on the seafloor, with geometries matching the ones formed in the analogue models (Fig. 11f). Salt tectonics is also active in part of the western sector (around 2°50') where the presence of a higher volume of salt could be related to a thicker deposition (i.e. the base of the salt was already deeper at the moment of the deposition, so a higher volume of salt has deposited there) or to a localized salt supply consequence of gravity gliding from surrounding areas.

5.3. Minibasins position

The minibasins are particularly well developed on the lower slope, where parts of them are still active (Fig. 8). As evidenced through numerical modelling (e.g. Peel, 2014), a single seed minibasin can trigger the formation of a serie of minibasins. This shows how difficult it can be to identify the main driver of the interpreted minibasins geometries in an area, especially when multiple factors are co-acting. Considering that density inversion was most likely absent at the beginning of the salt deformation in the area, other factors can be considered to be at the origin of minibasins formation: the presence of a slope, the compressional stress and the differential sedimentary load (Peel, 2014). In our study area, the base of the MU has multiple slope directions (Fig. 8a), both from the margin and from the uplifted plateau to the deeper basin, and the polygonal minibasins position also corresponds to the compressional domain of salt tectonics (Fig. 7c). We suggest that the greater development of minibasins in the western sector is at first order the result of these multiple slope directions and of the intersection between different zones of shortening: the downslope flow of salt inflates the diapirs separating the minibasins, supplying them with viscous evaporites, as already interpreted in other study areas (Rowan, 2023). The sedimentary loading is another potential element for the minibasins formation to be considered on the Algerian margin. As visible in Fig. 8, the salt diapirs are more developed at the external limit of the sedimentary load of the Algiers Ridge (Babonneau et al., 2017), where the pressure on the salt is lower. A partial contribution of the Algiers deep-sea fan in the determination of the position of salt diapirs development cannot be excluded, but also thanks to the produced analogue models it is clear that the minibasins form naturally even without the presence of a localized sedimentary overload.

6. Concluding remarks

In this study, we use the central Algerian margin as a case study to decipher the complex interplay between Messinian salt tectonics and slow-rate tectonic inversion of a passive margin in a stage of subduction initiation. The geophysical data interpretation, particularly the analysis of the geometry of the salt structures and the distribution and internal reflectors geometries of the brittle cover, allowed us to reconstruct the timing and mechanisms of salt tectonics. Comparing these findings to the produced analogue models helped corroborate the formulated hypotheses and understand the effect of the positive structural inversion of this margin on salt deformation. Distribution and geometry of the salt structures have been used as proxies to decipher crustal movements, often not well imaged in the seismic sections due to the screening effect of the halite on the seismic data and hidden by the ductile behaviour of the salt. Salt tectonics started early in all the area, possibly before the end of the Messinian Salinity Crisis, both by downbuilding and by gravity gliding resulting from low-rate crustal shortening and differential subsidence. A first phase of early and ubiquitous development of salt structures by downbuilding was followed by the tectonic uplift of a plateau at the margin toe, which led to the migration of part of the salt towards the deeper western sector by gravity gliding and to a slowdown of the salt deformation above the plateau. Salt walls of considerable thickness developed, and thick minibasins deposited, with the most developed polygonal minibasins located at the external limit of the Algiers fan, indicating a likely contribution of gravity spreading on salt deformation. Nowadays, the salt structures are active only where the relationship between salt and overburden thickness is favorable, and classical polygonal minibasins geometries are still recognized on the seafloor.

Finally, we note that by contrast with the other segments off Algeria (Hamai et al., 2018; Leffondré et al., 2021; Klingelhoefer et al., 2022), the effect of the tectonic inversion of the central Algerian margin is mostly expressed by a large plateau uplift, while no clear effect on the geometries of the salt structures (e.g. squeezing, minibasins deformation) has been imaged in our data. This is especially quite different from the narrow western Algerian margin where salt squeezing is widespread (Soto et al., 2022). This peculiarity is likely related to the northernmost position of the central Algerian margin relative to the Africa-Eurasia plate limit and to the stiffness of the Greater Kabylia metamorphic basement. We conclude that the rheological, geometrical and kinematic conditions play a key role on the way the salt behaves when exposed to crustal shortening.

CRediT authorship contribution statement

Gaia Travan: Writing – review & editing, Writing – original draft, Methodology, Investigation, Conceptualization. **Virginie Gaullier:** Writing – review & editing, Methodology, Investigation, Funding acquisition, Conceptualization. **Jacques Déverchère:** Writing – review & editing, Funding acquisition, Data curation. **Bruno C. Vendeville:** Methodology, Investigation, Conceptualization.

Declaration of competing interest

The authors declare that they have no known competing financial interests or personal relationships that could have appeared to influence the work reported in this paper.

Data availability

The authors do not have permission to share data.

Acknowledgments

References

Abbassene, F., Chazot, G., Bellon, H., Bruguier, O., Ouabadi, A., Maury, R.C., Déverchére, J., Bosch, D., Monié, P., 2016. A 17Ma onset for the post-collisional K-rich calc-alkaline magmatism in the Maghrebides: evidence from Bougaroun (northeastern Algeria) and geodynamic implications. Tectonophysics 674, 114–134. https://doi.org/10.1016/j.tecto.2016.02.013.

Aïdi, C., Beslier, M.-O., Yelles-Chaouche, A.K., Klingelhoefer, F., Bracene, R., Galve, A., Bounif, A., Schenini, L., Hamai, L., Schnurle, P., Djellit, H., Sage, F., Charvis, P., Déverchère, J., 2018. Deep structure of the continental margin and basin off Greater Kabylia, Algeria – new insights from wide-angle seismic data modeling and multichannel seismic interpretation. Tectonophysics 728–729, 1–22. https://doi.org/10.1016/j.tecto.2018.01.007.

Andreetto, F., Aloisi, G., Raad, F., Heida, H., Flecker, R., Agiadi, K., Lofi, J., Blondel, S., Bulian, F., Camerlenghi, A., Caruso, A., Ebner, R., Garcia-Castellanos, D., Gaullier, V., Guibourdenche, L., Gvirtzman, Z., Hoyle, T.M., Meijer, P.T., Moneron, J., Sierro, F.J., Travan, G., Tzevahirtzian, A., Vasiliev, I., Krijgsman, W., 2021. Freshening of the mediterranean salt giant: controversies and certainties around the terminal (upper Gypsum and lago-mare) phases of the messinian salinity crisis. Earth Sci. Rev. 216, 103577 https://doi.org/10.1016/j.earscirev.2021.103577.

Auzemery, A., Willingshofer, E., Sokoutis, D., Brun, J.P., Cloetingh, S.A.P.L., 2021. Passive margin inversion controlled by stability of the mantle lithosphere. Tectonophysics 817, 229042. https://doi.org/10.1016/j.tecto.2021.229042.

Auzende, J.M., Olivet, J.L., Bonnin, J., 1972. Une structure compressive au nord de l'Algérie? Deep Sea Res. Oceanogr. Abstr. 19, 149–155. https://doi.org/10.1016/0011-7471(72)90047-2.

Auzende, J.-M., Bonnin, J., Olivet, J.-L., 1975. La marge nord-africaine considérée comme marge active. Bull. Société Géologique Fr 17, 486–495.

Ayadi, A., Dorbath, C., Ousadou, F., Maouche, S., Chikh, M., Bounif, M.A., Meghraoui, M., 2008. Zemmouri earthquake rupture zone (Mw 6.8, Algeria): aftershocks sequence relocation and 3D velocity model. J. Geophys. Res. Solid Earth 113. https://doi.org/10.1029/2007JB005257.

Babonneau, N., Cattaneo, A., Savoye, B., Barjavel, G., Déverchère, J., Yelles, K., 2012. The kramis deep-sea fan off western Algeria: role of sediment waves in turbiditic levee growth. In: Prather, B.E., Deptuck, M.E., Mohrig, D., Hoorn, B.V., Wynn, R.B. (Eds.), Application of the Principles of Seismic Geomorphology to Continental Slope and Base-Of-Slope Systems: Case Studies from SeaFloor and Near-Sea Floor Analogues. SEPM Society for Sedimentary Geology. https://doi.org/10.1007/s00531-008-0373-5, 0.

Babonneau, N., Cattaneo, A., Ratzov, G., Déverchère, J., Yelles-Chaouche, A., Lateb, T., Bachir, R.S., 2017. Turbidite chronostratigraphy off Algiers, central Algerian margin: a key for reconstructing Holocene paleo-earthquake cycles. Mar. Geol., Subaquatic paleoseismology: records of large Holocene earthquakes in marine and lacustrine sediments 384, 63–80. https://doi.org/10.1016/j.margeo.2016.10.017.

Bache, F., Popescu, S.-M., Rabineau, M., Gorini, C., Suc, J.-P., Clauzon, G., Olivet, J.-L., Rubino, J.-L., Melinte-Dobrinescu, M.C., Estrada, F., Londeix, L., Armijo, R., Meyer, B., Jolivet, L., Jouannic, G., Leroux, E., Aslanian, D., Reis, A.T.D., Mocochain, L., Dumurdžanov, N., Zagorchev, I., Lesić, V., Tomić, D., Çağatay, M.N., Brun, J.-P., Sokoutis, D., Csato, I., Ucarkus, G., Çakır, Z., 2012. A two-step process for the reflooding of the Mediterranean after the Messinian Salinity Crisis. Basin Res. 24, 125–153. https://doi.org/10.1111/j.1365-2117.2011.00521.x.

Bellucci, M., Aslanian, D., Moulin, M., Rabineau, M., Leroux, E., Pellen, R., Poort, J., Del Ben, A., Gorini, C., Camerlenghi, A., 2021. Salt morphologies and crustal segmentation relationship: new insights from the Western Mediterranean Sea. Earth Sci. Rev. 222, 103818 https://doi.org/10.1016/j.earscirev.2021.103818.

Besème, G., 2013. Déformation salifère sur de hauts socles. Rapport de Stage de Master 1, 31. Univ. Lille 1, Parcours environnement.

Billi, A., Faccenna, C., Bellier, O., Minelli, L., Neri, G., Piromallo, C., Presti, D., Scrocca, D., Serpelloni, E., 2011. Recent tectonic reorganization of the Nubia-Eurasia convergent boundary heading for the closure of the western Mediterranean. Bull. Société Géologique Fr 182, 279–303. https://doi.org/10.2113/gssgfbull.182.4.279.

Blondel, S., Bellucci, M., Evans, S., Ben, A.D., Camerlenghi, A., 2022. Contractional salt deformation in a recently inverted basin: Miocene to current salt deformation within the central Algerian basin. Basin Res. 34, 1632–1654. https://doi.org/10.1111/bre.12673.

Booth-Rea, G., Gaidi, S., Melki, F., Marzougui, W., Azañón, J.M., Zargouni, F., Galvé, J. P., Pérez-Peña, J.V., 2018a. Late Miocene extensional collapse of northern Tunisia. Tectonics 37, 1626–1647. https://doi.org/10.1029/2017TC004846.

Booth-Rea, G., R. Ranero, C., Grevemeyer, I., 2018b. The Alboran volcanic-arc modulated the Messinian faunal exchange and salinity crisis. Sci. Rep. 8, 13015 https://doi.org/10.1038/s41598-018-31307-7.

Bougrine, A., Yelles-Chaouche, A.K., Calais, E., 2019. Active deformation in Algeria from continuous GPS measurements. Geophys. J. Int. 217, 572–588. https://doi.org/10.1093/gji/ggz035.

Burollet, P.F., Said, A., Trouvé, P., 1978. Slim holes drilled on the Algerian shelf. In: Hsü, K.J., et al. (Eds.), Initial Reports of the Deep Sea Drilling Project, Vol. 42, Part 2. Natl. Sci. Found., pp. 1181–1184. Washington, D.C.

Camerlenghi, A., Del Ben, A., Hübscher, C., Forlin, E., Geletti, R., Brancatelli, G., Micallef, A., Saule, M., Facchin, L., 2020. Seismic markers of the Messinian salinity crisis in the deep Ionian Basin. Basin Res. 32, 716–738. https://doi.org/10.1111/bre.12392.

Carminati, E., Doglioni, C., Gelabert, B., Panza, G.F., Raykova, R.B., Roca, E., Sabat, F., Scrocca, D., 2012. Evolution of the western mediterranean. In: Regional Geology and Tectonics: Phanerozoic Passive Margins, Cratonic Basins and Global Tectonic Maps. Elsevier, pp. 436–470. https://doi.org/10.1016/B978-0-444-56357-6.00011-1.

Cattaneo, A., Babonneau, N., Dan, G., Déverchère, J., Domzig, A., Gaullier, V., Lepillier, B., de Lépinay, B.M., Nouguès, A., Strzerzynski, P., Sultan, N., Yelles, K., 2010. Submarine landslides along the Algerian margin: a review of their occurrence and potential link with tectonic structures. In: Mosher, D.C., Shipp, R.C., Moscardelli, L., Chaytor, J.D., Baxter, C.D.P., Lee, H.J., Urgeles, R. (Eds.), Submarine Mass Movements and Their Consequences, Advances in Natural and Technological Hazards Research, vol. 28. Springer, Netherlands, Dordrecht, pp. 515–525. https://doi.org/10.1007/978-90-481-3071-9_42.

Cherchi, A., Montadert, L., 1982. Oligo-miocene rift of Sardinia and the early history of the western mediterranean basin. Nature 298, 736–739. https://doi.org/10.1038/298736a0.

Chertova, M.V., Spakman, W., van den Berg, A.P., van Hinsbergen, D.J.J., 2014. Absolute plate motions and regional subduction evolution. G-cubed 15, 3780–3792. https://doi.org/10.1002/2014GC005494.

CIESM, 2008. The Messinian Salinity Crisis from mega-deposits to microbiology - a consensus report. N° 33, 2008. In: Briand, F. (Ed.), CIESM Workshop Monographs, p. 168. Monaco.

Clauzon, G., Suc, J.-P., Popescu, S.-M., Melinte-Dobrinescu, M.C., Quillévéré, F., Warny, S.A., Fauquette, S., Armijo, R., Meyer, B., Rubino, J.-L., Lericolais, G., Gillet, H., Çağatay, M.N., Ucarkus, G., Escarguel, G., Jouannic, G., Dalesme, F., 2008. Chronology of the Messinian events and paleogeography of the Mediterranean regions s.l. CIESM 2008. The Messinian Salinity Crisis from Mega-Deposits to Microbiology - A Consensus Report 33, 168.

Cope, M.J., 2003. Algerian licensing round may offer opportunity for exploration plays in deep offshore frontier. First Break 21. https://doi.org/10.3997/1365-2397.21.7.25550.

Cornée, J.-J., Maillard, A., Conesa, G., Garcia, F., Saint Martin, J.-P., Sage, F., Münch, P., 2008. Onshore to offshore reconstruction of the Messinian erosion surface in Western Sardinia, Italy: implications for the Messinian salinity crisis. Sediment. Geol. 210, 48–60. https://doi.org/10.1016/j.sedgeo.2008.06.005.

Dal Cin, M., Del Ben, A., Mocnik, A., Accaino, F., Geletti, R., Wardell, N., Zgur, F., Camerlenghi, A., 2016. Seismic imaging of late Miocene (messinian) evaporites from western mediterranean back-arc basins. Petrol. Geosci. 22, 297–308. https://doi.org/10.1144/petgeo2015-096.

Dan-Untersesh, G., Sultan, N., Savoye, B., Deverchere, J., Yelles, K., 2009. Quantifying the role of sandy-silty sediments in generating slope failures during earthquakes: example from the Algerian margin. Int. J. Earth Sci. 98, 769–789. https://doi.org/10.1007/s00531-008-0373-5.

Dan-Untersesh, G., Savoye, B., Gaullier, V., Cattaneo, A., Déverchère, J., Yelles-Chaouche, A., 2011. Algerian margin sedimentation patterns (Algiers area, southwestern mediterranean). In: Mass-Transport Deposits in Deepwater Settings. SEPM Special Publication, Edition, pp. 69–84. https://doi.org/10.2110/sepmsp.096.069.

Déverchère, J., 2003. MARADJA cruise, RV le suroît, French oceanographic cruises, SISMER data base. https://doi.org/10.17600/3020100.

Déverchère, J., Yelles, K., Domzig, A., de Lépinay, B.M.D., J,p, B., Gaullier, V., Bracène, R., Calais, E., Bruno, S., Kherroubi, A., Roy, P., H, P., Dan-Untersesh, G., 2005a. Active thrust faulting offshore Boumerdes, Algeria, and its relations to the 2003 Mw 6.9 earthquake. Geophys. Res. Lett. 32, L04311 https://doi.org/10.1029/2004GL021646.

Déverchère, J., Yelles, K., Domzig, A., Lépinay, B.M.D., Cattaneo, A., Gaullier, V., Kherroubi, A., 2005b. Overall tectonic pattern of the Algerian margin: evidences for active folding and thrusting from the 2003 and 2005 MARADJA cruises 1. CIESM Congress 38, 82.

Déverchère, J., Barbé, A., Kernec, M., Jaud, M., Ruault, R., 2022. A submarine morphotectonic analysis combining GIS-based methods and virtual reality: case study of the low-rate active thrust faulting off Boumerdès (Algeria). Front. Earth Sci. 10, Research Topic: Geoscientific Visualization in Solid Earth Geophysics. https://doi.org/10.3389/feart.2022.1010226.

Domzig, A., Yelles, K., Le Roy, C., Déverchère, J., Bouillin, J.-P., Bracène, R., Mercier de Lépinay, B., Le Roy, P., Calais, E., Kherroubi, A., Gaullier, V., Savoye, B., Pauc, H., 2006. Searching for the Africa–Eurasia Miocene boundary offshore western Algeria

(MARADJA'03 cruise). Compt. Rendus Geosci. 338, 80–91. https://doi.org/10.1016/j.crte.2005.11.009.

Domzig, A., Gaullier, V., Giresse, P., Pauc, H., Déverchère, J., Yelles, K., 2009. Deposition processes from echo-character mapping along the western Algerian margin (Oran–Tenes), Western Mediterranean. Mar. Petrol. Geol. 26, 673–694. https://doi.org/10.1016/j.marpetgeo.2008.05.006.

Driussi, O., Maillard, A., Ochoa, D., Lofi, J., Chanier, F., Gaullier, V., Briais, A., Sage, F., Sierro, F., Garcia, M., 2015. Messinian Salinity Crisis deposits widespread over the Balearic Promontory: insights from new high-resolution seismic data. Mar. Pet. Geol., The Messinian events and hydrocarbon exploration in the Mediterranean 66, 41–54. https://doi.org/10.1016/j.marpetgeo.2014.09.008.

Eisenstadt, G., Vendeville, B.C., Withjack, M.O., 1997. Experimental Modeling of Tectonic Processes. Course Notes. American Association of Petroleum Geologists Student Chapter course #19, p. 146.

Frizon de Lamotte, D., Saint Bezar, B., Bracène, R., Mercier, E., 2000. The two main steps of the Atlas building and geodynamics of the western Mediterranean. Tectonics 19, 740–761. https://doi.org/10.1029/2000TC900003.

Garcia-Castellanos, D., Estrada, F., Jiménez-Munt, I., Gorini, C., Fernàndez, M., Vergés, J., De Vicente, R., 2009. Catastrophic flood of the Mediterranean after the Messinian salinity crisis. Nature 462, 778–781. https://doi.org/10.1038/nature08555.

Gaullier, V., Chanier, F., Lymer, G., Vendeville, B.C., Maillard, A., Thinon, I., Lofi, J., Sage, F., Loncke, L., 2014. Salt tectonics and crustal tectonics along the Eastern Sardinian margin, Western Tyrrhenian: new insights from the "METYSS 1" cruise. Tectonophysics 615–616, 69–84. https://doi.org/10.1016/j.tecto.2013.12.015.

Gaullier, V., Vendeville, B.C., 2005. Salt tectonics driven by sediment progradation: Part II—Radial spreading of sedimentary lobes prograding above salt. AAPG Bull 89, 1081–1089. https://doi.org/10.1306/03310503064.

Gearing, P., Gearing, J.N., Lytle, T.F., Lytle, J.S., 1976. Hydrocarbons in 60 northeast Gulf of Mexico shelf sediments: a preliminary survey. Geochem. Cosmochim. Acta 40, 1005–1017. https://doi.org/10.1016/0016-7037(76)90043-0.

Giresse, P., Pauc, H., Déverchère, J., 2009. Sedimentary processes and origin of sediment gravity-flow deposits on the western Algerian margin during late Pleistocene and Holocene. Mar. Petrol. Geol. 26, 695–710. https://doi.org/10.1016/j.marpetgeo.2008.03.011.

Giresse, P., Bassetti, M.-A., Pauc, H., Gaullier, V., Déverchère, J., Bracene, R., Yelles, A., 2013. Sediment accumulation rates and turbidite frequency in the eastern Algerian margin. An attempt to examine the triggering mechanisms. Sediment. Geol. 294, 266–281. https://doi.org/10.1016/j.sedgeo.2013.06.005.

Gorini, C., Marrec, A.L., Mauffret, A., 1993. Contribution to the structural and sedimentary history of the Gulf of Lions (western Mediterranean) from the ECORS profiles, industrial seismic profiles and well data. Bull. Société Géologique Fr 164, 353–363.

Gorini, C., Montadert, L., Rabineau, M., 2015. New imaging of the salinity crisis: dual Messinian lowstand megasequences recorded in the deep basin of both the eastern and western Mediterranean. Mar. Pet. Geol., The Messinian events and hydrocarbon exploration in the Mediterranean 66, 278–294. https://doi.org/10.1016/j.marpetgeo.2015.01.009.

Govers, R., Meijer, P., Krijgsman, W., 2009. Regional isostatic response to messinian salinity crisis events. Tectonophysics 463, 109–129. https://doi.org/10.1016/j.tecto.2008.09.026.

Granado, P., Urgeles, R., Sàbat, F., Albert-Villanueva, E., Roca, E., Muñoz, J.A., Mazzuca, N., Gambini, R., 2016. Geodynamical framework and hydrocarbon plays of a salt giant: the NW Mediterranean Basin. Pet. Geosci. 22, 309–321. https://doi.org/10.1144/petgeo2015-084.

Haidar, S., Déverchère, J., Graindorge, D., Arab, M., Medaouri, M., Klingelhoefer, F., 2022. Back-Arc dynamics controlled by slab rollback and tearing: a reappraisal of seafloor spreading and kinematic evolution of the eastern Algero-Balearic Basin (western mediterranean) in the middle-late Miocene. Tectonics 41, e2021TC006877. https://doi.org/10.1029/2021TC006877.

Hamai, L., Petit, C., Abtout, A., Yelles-Chaouche, A., Déverchère, J., 2015. Flexural behaviour of the north Algerian margin and tectonic implications. Geophys. J. Int. 201, 1426–1436. https://doi.org/10.1093/gji/ggv098.

Hamai, L., Petit, C., Le Pourhiet, L., Yelles-Chaouche, A., Déverchère, J., Beslier, M.-O., Abtout, A., 2018. Towards subduction inception along the inverted North African margin of Algeria? Insights from thermo-mechanical models. Earth Planet Sci. Lett. 501, 13–23. https://doi.org/10.1016/j.epsl.2018.08.028.

Heida, H., Raad, F., Garcia-Castellanos, D., Jiménez- Munt, I., Maillard, A., Lofi, J., 2022. Flexural-isostatic reconstruction of the western mediterranean during the messinian salinity crisis: implications for water level and basin connectivity. Basin Res. 34, 50–80. https://doi.org/10.1111/bre.12610.

Hsü, K.J., Montadert, L., 1978. Initial Rep. Deep Sea Drill. Proj. 42 (Pt. 1), 42 Pt. 1.

Hsü, K.J., Cita, M.B., Ryan, W.B.F., 1973. The Origin of the Mediterranean Evaporites. U. S. Govt. Printing Office, Washington DC.

Hubbert, M.K., 1937. Theory of scale models as applied to the study of geologic structures. Geol. Soc. Am. Bull. 1459–1520.

Jolivet, L., Faccenna, C., 2000. Mediterranean extension and the Africa-Eurasia collision. Tectonics 19, 1095–1106. https://doi.org/10.1029/2000TC900018.

Jolivet, L., Augier, R., Robin, C., Suc, J.-P., Rouchy, J.M., 2006. Lithospheric-scale geodynamic context of the Messinian salinity crisis. Sediment. Geol. 188–189, 9–33. https://doi.org/10.1016/j.sedgeo.2006.02.004.

Jolivet, L., Baudin, T., Calassou, S., Chevrot, S., Ford, M., Issautier, B., Lasseur, E., Masini, E., Manatschal, G., Mouthereau, F., Thinon, I., Vidal, O., 2021. Geodynamic evolution of a wide plate boundary in the Western Mediterranean, near-field versus far-field interactions. BSGF - Earth Sci. Bull. 192, 48. https://doi.org/10.1051/bsgf/2021043.

Jones, I.F., Davison, I., 2014. Seismic imaging in and around salt bodies. Interpretation 2 (1), SL1–SL20. https://doi.org/10.1190/INT-2014-0033.

Kherroubi, A., Déverchère, J., Yelles, A., Mercier de Lépinay, B., Domzig, A., Cattaneo, A., Bracène, R., Gaullier, V., Graindorge, D., 2009. Recent and active deformation pattern off the easternmost Algerian margin, Western Mediterranean Sea: new evidence for contractional tectonic reactivation. Mar. Geol. 261, 17–32. https://doi.org/10.1016/j.margeo.2008.05.016.

Kherroubi, A., Yelles-Chaouche, A., Koulakov, I., Déverchère, J., Beldjoudi, H., Haned, A., Semmane, F., Aidi, C., 2017. Full aftershock sequence of the Mw 6.9 2003 boumerdes earthquake, Algeria: space–time distribution, local tomography and seismotectonic implications. Pure Appl. Geophys. 174, 2495–2521. https://doi.org/10.1007/s00024-017-1571-5.

Klingelhoefer, F., Déverchère, J., Graindorge, D., Aïdi, C., Badji, R., Bouyahiaoui, B., Leprêtre, A., Mihoubi, A., Beslier, M.-O., Charvis, P., Schnurle, P., Sage, F., Medaouri, M., Arab, M., Bracene, R., Yelles-Chaouche, A., Badsi, M., Galvé, A., Géli, L., 2022. Formation, segmentation and deep crustal structure variations along the Algerian margin from the SPIRAL seismic experiment. J. Afr. Earth Sci. 186, 104433 https://doi.org/10.1016/j.jafrearsci.2021.104433.

Krijgsman, W., Hilgen, F.J., Raffi, I., Sierro, F.J., Wilson, D.S., 1999. Chronology, causes and progression of the Messinian salinity crisis. Nature 400, 652–655. https://doi.org/10.1038/23231.

Kumar, A., Fernàndez, M., Vergés, J., Torne, M., Jiménez-Munt, I., 2021. Opposite symmetry in the lithospheric structure of the alboran and Algerian basins and their margins (western mediterranean): geodynamic implications. J. Geophys. Res. Solid Earth 126, e2020JB021388. https://doi.org/10.1029/2020JB021388.

LeCompte, P., 1965. Creep in rock salt. J. Geol. 73, 469–484.

Leffondré, P., Déverchère, J., Medaouri, M., Klingelhoefer, F., Graindorge, D., Arab, M., 2021. Ongoing inversion of a passive margin: spatial variability of strain markers along the Algerian margin and basin (Mediterranean Sea) and seismotectonic implications. Front. Earth Sci. 9 https://doi.org/10.3389/feart.2021.674584.

Leprêtre, A., Klingelhoefer, F., Graindorge, D., Schnurle, P., Beslier, M.O., Yelles, K., Déverchère, J., Bracene, R., 2013. Multiphased tectonic evolution of the Central Algerian margin from combined wideangle and reflection seismic data off Tipaza. Algeria. J. Geophys. Res. Solid Earth 118, 3899–3916. https://doi.org/10.1002/jgrb.50318,2013.

Leprêtre, A., Lamotte, D.F. de, Combier, V., Gimeno-Vives, O., Mohn, G., Eschard, R., 2018. The Tell-Rif orogenic system (Morocco, Algeria, Tunisia) and the structural heritage of the southern Tethys margin. BSGF - Earth Sci. Bull. 189, 10. https://doi.org/10.1051/bsgf/2018009.

Lofi, J., 2018. Seismic Atlas of the Messinian Salinity Crisis markers in the Mediterranean Sea - Volume 2, Mémoires de la Société Géologique de France. Société Géologique de France.

Lofi, J., Gorini, C., Berné, S., Clauzon, G., Tadeu Dos Reis, A., Ryan, W.B.F., Steckler, M. S., 2005. Erosional processes and paleo-environmental changes in the western gulf of Lions (SW France) during the messinian salinity crisis. Mar. Geol. 217, 1–30. https://doi.org/10.1016/j.margeo.2005.02.014.

Lofi, J., Déverchère, J., Gaullier, V., Herve, G., Gorini, C., Guennoc, P., Loncke, L., Maillard, A., Sage, F., Thinon, I., 2011a. Seismic Atlas of the Messinian Salinity Crisis Markers in the Mediterranean and Black Seas, Mém. Soc. Géol. Fr., n.s., 179, and World Geological Map Commission, p. 72.

Lofi, J., Sage, F., Déverchère, J., Loncke, L., Maillard, A., Gaullier, V., Thinon, I., Gillet, H., Guennoc, P., Gorini, C., 2011b. Refining our knowledge of the Messinian salinity crisis records in the offshore domain through multi-site seismic analysis. Bull. Société Géologique Fr 182, 163–180. https://doi.org/10.2113/gssgfbull.182.2.163.

Lugli, S., 1997. The Realmonte salt deposit (Agrigento, Sicily): geology and exploitation. In: Neogene Mediterranean Paleoceanography. Società Geologica Italiana, pp. 44–60.

Lymer, G., 2010. Interaction entre tectonique crustale compressive et tectonique salifère gravitaire sur la marge nord-algérienne : analyse de données sismiques, bathymétriques et modélisation analogique. Rapport de stage de Master 2, Univ. Lille 1 et UPVD, Parcours GEMSED, p. 41.

Lymer, G., Vendeville, B.C., Gaullier, V., Chanier, F., Gaillard, M., 2018. Using salt tectonic structures as proxies to reveal post-rift crustal tectonics: the example of the Eastern Sardinian margin (Western Tyrrhenian Sea). Mar. Petrol. Geol. 96, 214–231. https://doi.org/10.1016/j.marpetgeo.2018.05.037.

Macchiavelli, C., Vergés, J., Schettino, A., Fernàndez, M., Turco, E., Casciello, E., Torne, M., Pierantoni, P.P., Tunini, L., 2017. A new southern north atlantic isochron map: insights into the drift of the iberian plate since the late cretaceous. J. Geophys. Res. Solid Earth 122, 9603–9626. https://doi.org/10.1002/2017JB014769.

Mahsas, A., Lammali, K., Yelles, K., Calais, E., Freed, A.M., Briole, P., 2008. Shallow afterslip following the 2003 may 21, Mw= 6.9 boumerdes earthquake, Algeria. Geophys. J. Int. 172, 155–166. https://doi.org/10.1111/j.1365-246X.2007.03594.x.

Maillard, A., Gaullier, V., Vendeville, B.C., Odonne, F., 2003. Influence of differential compaction above basement steps on salt tectonics in the Ligurian-Provençal Basin, northwest Mediterranean. Mar. Petrol. Geol. 20, 13–27. https://doi.org/10.1016/S0264-8172(03)00022-9.

Maillard, A., Gorini, C., Mauffret, A., Sage, F., Lofi, J., Gaullier, V., 2006. Offshore evidence of polyphase erosion in the Valencia Basin (northwestern mediterranean): scenario for the messinian salinity crisis. Sediment. Geol., The Messinian Salinity Crisis Revisited 188–189, 69–91. https://doi.org/10.1016/j.sedgeo.2006.02.006.

Maillard, A., Gaullier, V., Lézin, C., Chanier, F., Odonne, F., Lofi, J., 2020. New onshore/offshore evidence of the messinian erosion surface from key areas: the ibiza-balearic promontary and the orosei-eastern tyrrhenian margin. BSGF – Earth Sciences Bulletin 191, 9. https://doi.org/10.1051/bsgf/2020007.

Manzi, V., Lugli, S., Lucchi, F.R., Roveri, M., 2005. Deep-water clastic evaporites deposition in the Messinian Adriatic foredeep (northern Apennines, Italy): did the Mediterranean ever dry out? Sedimentology 52, 875–902. https://doi.org/10.1111/j.1365-3091.2005.00722.x.

Mauffret, A., 2007. The northwestern (maghreb) boundary of the Nubia (Africa) plate. Tectonophysics 429, 21–44. https://doi.org/10.1016/j.tecto.2006.09.007.

Mauffret, A., Frizon de Lamotte, D., Lallemant, S., Gorini, C., Maillard, A., 2004. E-W opening of the Algerian basin (western mediterranean). Terra. Nova 16, 257–264. https://doi.org/10.1111/j.1365-3121.2004.00559.x.

Medaouri, M., Déverchère, J., Graindorge, D., Bracene, R., Badji, R., Ouabadi, A., Yelles-Chaouche, K., Bendiab, F., 2014. The transition from Alboran to Algerian basins (Western Mediterranean Sea): chronostratigraphy, deep crustal structure and tectonic evolution at the rear of a narrow slab rollback system. J. Geodyn. 77, 186–205. https://doi.org/10.1016/j.jog.2014.01.003. SI : Geodynamic evolution of the Alboran domain.

Nesteroff, W.D., 1973. Un modèle pour les evaporites messiniennes en Méditerranée: des bassins peu profonds avec des dépots d'évaporites lagunaires. In: Drooger, C.W., et al. (Eds.), Messinian Events in the Mediterranean, pp. 68–81.

Nocquet, J.-M., Calais, E., 2004. Geodetic measurements of crustal deformation in the western mediterranean and Europe. Pure Appl. Geophys. 161, 661–681. https://doi.org/10.1007/s00024-003-2468-z.

Obone-Zue-Obame, E.M., Gaullier, V., Sage, F., Maillard, A., Lofi, J., Vendeville, B., Thinon, I., Réhault, J.-P., 2011. The sedimentary markers of the Messinian salinity crisis and their relation with salt tectonics on the Provençal margin (western Mediterranean): results from the "MAURESC" cruise. Bull. Société Géologique Fr 182, 181–196. https://doi.org/10.2113/gssgfbull.182.2.181.

Orszag-Sperber, F., 2006. Changing perspectives in the concept of "lago-mare" in mediterranean late Miocene evolution. Sediment. Geol., The Messinian Salinity Crisis Revisited 188–189, 259–277. https://doi.org/10.1016/j.sedgeo.2006.03.008.

Ousadou, F., Bezzeghoud, M., 2019. Seismicity of the Algerian Tell atlas and the impacts of major earthquakes. In: Bendaoud, A., Hamimi, Z., Hamoudi, M., Djemai, S., Zoheir, B. (Eds.), The Geology of the Arab World—An Overview. Springer Geology. Springer International Publishing, Cham, pp. 401–426. https://doi.org/10.1007/978-3-319-96794-3_11.

Peel, F.J., 2014. How do salt withdrawal minibasins form? Insights from forward modelling, and implications for hydrocarbon migration. Tectonophysics 630, 222–235. https://doi.org/10.1016/j.tecto.2014.05.027.

Piqué, A., Aït Brahim, L., El Azzouzi, M., Maury, R.C., Bellon, H., Semroud, B., Laville, E., 1998. Le poinçon maghrébin: contraintes structurales et géochimiques, Comptes Rendus Académie des Sciences, Series IIA - Earth Planet. Science 326 (8), 575–581. https://doi.org/10.1016/S1251-8050(98)80209-7.

Rabineau, M., Leroux, E., Aslanian, D., Bache, F., Gorini, C., Moulin, M., Molliex, S., Droz, L., dos Reis, A.T., Rubino, J.L., Guillocheau, F., Olivet, J.L., 2014. Quantifying subsidence and isostatic readjustment using sedimentary paleomarkers, example from the Gulf of Lion. Earth Planet Sci. Lett. 388, 353–366. https://doi.org/10.1016/j.epsl.2013.11.059.

Ratzov, G., Cattaneo, A., Babonneau, N., Déverchère, J., Yelles, K., Bracene, R., Courboulex, F., 2015. Holocene turbidites record earthquake supercycles at a slow-rate plate boundary. Geology 43, 331–334. https://doi.org/10.1130/G36170.1.

Recanati, A., Missenard, Y., Leprêtre, R., Gautheron, C., Barbarand, J., Abbassene, F., Abdallah, N., Ouabadi, A., Derder, M.E.M., Boukari, C., Pinna-Jamme, R., Haurine, F., 2019. A Tortonian onset for the Algerian margin inversion: evidence from low-temperature thermochronology. Terra. Nova 31, 39–48. https://doi.org/10.1111/ter.12367.

Réhault, J.-P., Boillot, G., Mauffret, A., 1984. The western mediterranean basin geological evolution. Mar. Geol., Geological and Geodynamical Aspects on the Mediterranean 55, 447–477. https://doi.org/10.1016/0025-3227(84)90081-1.

Roveri, M., Manzi, V., Bergamasco, A., Falcieri, F.M., Gennari, R., Lugli, S., Schreiber, B.C., 2014. Dense shelf water cascading and Messinian Canyons: a new scenario for the Mediterranean salinity crisis. Am. J. Sci. 314, 751–784. https://doi.org/10.2475/05.2014.03.

Rowan, M.G., 2023. Structural architecture and evolution of eastern Mississippi Canyon, northern gulf of Mexico. Mar. Petrol. Geol. 150, 106127 https://doi.org/10.1016/j.marpetgeo.2023.106127.

Ryan, W.B.F., Hsü, K.J., Cita, M.B., Dumitrica, P., Lort, J.M., Mayne, W., Nesteroff, W.D., Pautot, G., Stradner, H., Wezel, F.C., 1973. Initial reports of the deep sea drilling project. US Gov. Print. Off. Wash. 13, 32.

Ryan, W.B.F., Carbotte, S.M., Coplan, J., O'Hara, S., Melkonian, A., Arko, R., Weissel, R.A., Ferrini, V., Goodwillie, A., Nitsche, F., Bonczkowski, J., Zemsky, R., 2009. Global Multi-Resolution Topography (GMRT) synthesis data set. Geochem. Geophys. Geosyst. 10, Q03014 https://doi.org/10.1029/2008GC002332.

Savoye, B., Piper, D.J.W., 1991. The Messinian event on the margin of the Mediterranean Sea in the Nice area, southern France. Mar. Geol. 97, 279–304. https://doi.org/10.1016/0025-3227(91)90121-J.

Schellart, W.P., Strak, V., 2016. A review of analogue modelling of geodynamic processes: approaches, scaling, materials and quantification, with an application to subduction experiments. J. Geodyn., 200 years of geodynamic modelling 100, 7–32. https://doi.org/10.1016/j.jog.2016.03.009.

Schettino, A., Turco, E., 2006. Plate kinematics of the western mediterranean region during the Oligocene and early Miocene. Geophys. J. Int. 166, 1398–1423. https://doi.org/10.1111/j.1365-246X.2006.02997.x.

Schettino, A., Turco, E., 2011. Tectonic history of the western tethys since the late triassic. GSA Bull 123 (1), 89–105. https://doi.org/10.1130/B30064.

Selli, R., 1973. An outline of the Italian Messinian. In: Messinian Events in the Mediterranean, pp. 150–171.

Simm, R., Bacon, M., 2014. Seismic Amplitude. An Interpreters Handbook, 280. Cambridge University Press.

Soto, J.I., Déverchère, J., Hudec, M.R., Medaouri, M., Badji, R., Gaullier, V., Leffondré, P., 2022. Crustal structures and salt tectonics on the margins of the western Algerian Basin (Mediterranean Region). Mar. Petrol. Geol. 144, 105820 https://doi.org/10.1016/j.marpetgeo.2022.105820.

Stich, D., Serpelloni, E., de Lis Mancilla, F., Morales, J., 2006. Kinematics of the Iberia–Maghreb plate contact from seismic moment tensors and GPS observations. Tectonophysics 426, 295–317. https://doi.org/10.1016/j.tecto.2006.08.004.

Stich, D., Martin, R., Morales, J., López-Comino, J.-Á., Mancilla, F. de L., 2020. Slip partitioning in the 2016 alboran sea earthquake sequence (western mediterranean). Front. Earth Sci. 8, 587356 https://doi.org/10.3389/feart.2020.587356.

Strzerzynski, P., Déverchère, J., Cattaneo, A., Domzig, A., Yelles, K., Mercier de Lépinay, B., Babonneau, N., Boudiaf, A., 2010. Tectonic inheritance and Pliocene-Pleistocene inversion of the Algerian margin around Algiers: insights from multibeam and seismic reflection data: central Algerian margin inversion. Tectonics 29 (TC2008), 1–22. https://doi.org/10.1029/2009TC002547 n/a-n/a.

Strzerzynski, P., Dominguez, S., Boudiaf, A., Déverchère, J., 2021. Tectonic inversion and geomorphic evolution of the Algerian margin since messinian times: insights from new onshore/offshore analog modeling experiments. Tectonics 40, e2020TC006369. https://doi.org/10.1029/2020TC006369.

Tari, G., Connors, C., Flinch, J., Granath, J., Pace, P., Sobornov, K., Soto, J.I., 2023. Negative structural inversion: an overview. Mar. Petrol. Geol. 152, 106223 https://doi.org/10.1016/j.marpetgeo.2023.106223.

Travan, G., 2022. Interactions between salt tectonics and crustal tectonics in the Mediterranean and in the Barents Sea. PhD thesis. Université de Lille (France) 244.

van Hinsbergen, D.J.J., Vissers, R.L.M., Spakman, W., 2014. Origin and consequences of western Mediterranean subduction, rollback, and slab segmentation. Tectonics 33, 393–419. https://doi.org/10.1002/2013TC003349.

Vergés, J., Fernàndez, M., 2012. Tethys–atlantic interaction along the iberia–africa plate boundary: the betic–rif orogenic system. Tectonophysics, Orogenic processes and structural heritage in Alpine-type mountain belts 579, 144–172. https://doi.org/10.1016/j.tecto.2012.08.032.

Vergés, J., Sàbat, F., 1999. Constraints on the neogene mediterranean kinematic evolution along a 1000 km transect from Iberia to Africa. Geol. Soc. Lond. Spec. Publ. 156, 63–80. https://doi.org/10.1144/GSL.SP.1999.156.01.05.

Warren, J.K., 2010. Evaporites through time: tectonic, climatic and eustatic controls in marine and nonmarine deposits. Earth Sci. Rev. 98, 217–268. https://doi.org/10.1016/j.earscirev.2009.11.004.

Yelles, K., Lammali, K., Mahsas, A., Calais, E., Briole, P., 2004. Coseismic deformation of the may 21st, 2003, Mw = 6.8 boumerdes earthquake, Algeria, from GPS measurements. Geophys. Res. Lett. 31 https://doi.org/10.1029/2004GL019884.

Yelles, A., Domzig, A., Déverchère, J., Bracène, R., Mercier de Lépinay, B., Strzerzynski, P., Bertrand, G., Boudiaf, A., Winter, T., Kherroubi, A., Le Roy, P., Djellit, H., 2009. Plio-quaternary reactivation of the neogene margin off NW Algiers, Algeria: the khayr al Din bank. Tectonophysics 475, 98–116. https://doi.org/10.1016/j.tecto.2008.11.030.

Zhang, X., Liu, W., Chen, J., Jiang, D., Fan, J., Daemen, J.J.K., Qiao, W., 2022. Large-scale CO_2 disposal/storage in bedded rock salt caverns of China: an evaluation of safety and suitability. Energy 249, 123727 https://doi.org/10.1016/j.energy.2022.123727.